[18] Osada K, Oshima H, Kobayashi D, Doi M, Enoki M, Yamasaki Y, et al. Quantized folding of plasmid DNA condensed with block catiomer into characteristic rod structures promoting transgene efficacy. J Am Chem Soc 2010; 132:12343–8.
[19] Mishra S, Webster P, Davis ME. PEGylation significantly affects cellular uptake and intracellular trafficking of non-viral gene delivery particles. Eur J Cell Biol 2004;83:97–111.
[20] Kursa M, Walker GF, Roessler V, Ogris M, Roedl W, Kircheis R, et al. Novel shielded transferrin-polyethylene glycol-polyethylenimine/DNA complexes for systemic tumor-targeted gene transfer. Bioconjug Chem 2003;14: 222–31.
[21] Varkouhi AK, Scholte M, Storm G, Haisma HJ. Endosomal escape pathways for delivery of biologicals. J Control Release 2011;151:220–8.
[22] Mancuso A, Calabrò F, Sternberg CN. Current therapies and advances in the treatment of pancreatic cancer. Crit Rev Oncol Hematol 2006;58:231–41.
[23] Freelove R, Walling AD. Pancreatic cancer: diagnosis and management. Am Fam Physician 2006;73:485–92.
[24] Huguet F, Girard N, Guerche CS. Chemoradiotherapy in the management of locally advanced pancreatic carcinoma: a qualitative systematic review. J Clin Oncol 2009;27:2269–77.
[25] Klautke G, Brunner TB. Radiotherapy in pancreatic cancer. Strahlenther Onkol 2008;184:557–64.
[26] Zuckerman DS, Ryan DP. Adjuvant therapy for pancreatic cancer: a review. Cancer 2008;112:243–9.
[27] Folkman J, Bach M, Rowe JW, Davidoff F, Lambert P, Hirsch C, et al. Tumor angiogenesis-therapeutic implications. N Engl J Med 1971;285:1182–6.
[28] Quesada AR, Munoz-Chapuli R, Medina MA. Anti-angiogenic drugs: from bench to clinical trials. Med Res Rev 2006;26:483–530.
[29] Pralhad T, Madhusudan S, Rajendrakumar K. Concept mechanisms and therapeutics of angiogenesis in cancer and other diseases. J Pharm Pharmaco 2003;55:1045–53.
[30] Carmeliet P, Jain RK. Angiogenesis in cancer and other diseases. Nature 2000; 407:249–57.
[31] Kong HL, Hecht D, Song W, Kovesdi I, Hackett NR, Yayon A, et al. Regional suppression of tumor growth by in vivo transfer of a cDNA encoding a secreted form of the extracellular domain of the Flt-1 vascular endothelial growth factor receptor. Hum Gene Ther 1998;9:823–33.
[32] Oba M, Vachutinsky Y, Miyata K, Kano MR, Ikeda S, Nishiyama N, et al. Antiangiogenic gene therapy of solid tumor by systemic injection of polyplex micelles loading plasmid DNA encoding soluble Flt-1. Mol Pharm 2010;7: 501–9.
[33] Vachutinsky Y, Oba M, Miyata K, Hiki S, Kano MR, Nishiyama N, et al. Antiangiogenic gene therapy of experimental pancreatic tumor by sFlt-1 plasmid DNA carried by RGD-modified crosslinked polyplex micelles. J Control Release 2011;149:51–7.
[34] Cabral H, Matsumoto Y, Mizuno K, Chen Q, Murakami M, Kimura M, et al. Accumulation of sub-100 nm polymeric micelles in poorly permeable tumours depends on size. Nat Nanotech 2011;12:815–23.

Biomaterials 33 (2012) 325–332

Contents lists available at SciVerse ScienceDirect

Biomaterials

journal homepage: www.elsevier.com/locate/biomaterials

Enhanced gene expression promoted by the quantized folding of pDNA within polyplex micelles

Kensuke Osada[a,c], Tomonori Shiotani[a], Theofilus A. Tockary[a], Daigo Kobayashi[a], Hiroki Oshima[a], Sorato Ikeda[a], Ronald J. Christie[b,c], Keiji Itaka[b,c], Kazunori Kataoka[a,b,c,*]

[a] Department of Materials Engineering, Graduate School of Engineering, The University of Tokyo, 7-3-1 Hongo, Bunkyo-ku, Tokyo 113-8656, Japan
[b] Division of Clinical Biotechnology, Center for Disease Biology and Integrative Medicine, Graduate School of Medicine, The University of Tokyo, 7-3-1 Hongo, Bunkyo-ku, Tokyo 113-8656, Japan
[c] Center for NanoBio Integration, The University of Tokyo, 7-3-1 Hongo, Bunkyo-ku, Tokyo 113-8656, Japan

ARTICLE INFO

Article history:
Received 1 September 2011
Accepted 21 September 2011
Available online 10 October 2011

Keywords:
DNA
Micelle
Nanoparticle
Gene transfer
In vivo test
In vitro test

ABSTRACT

Selective packaging of plasmid DNA (pDNA) into folded rod or collapsed sphere structures in polyplex micelles was demonstrated by modulating the PLys segment length of poly(ethylene glycol)-*block*-poly(L-lysine) (PEG-PLys) block catiomers used for micelle formation. The two basic packaging structures correlated well to the integrity of double-stranded DNA contained within the micelles. Rod structures formed by the quantized folding mechanism, which results in dissociation of double-stranded DNA only at each fold. Collapsed sphere structures formed by substantial random disruption of the double-stranded DNA structure. Analysis of gene expression in a cell-free transcription/translation system, cultured cells and also skeletal muscle of mice showed that micelles containing pDNA packaged by quantized folding exhibited higher gene expression than naked pDNA and micelles containing collapsed pDNA. These results indicate that controlled packaging of pDNA into an appropriate structure is critical for achieving effective gene expression. Improved gene transfection and expression resulting from the quantized folding of pDNA within polyplex micelles is promising for application in therapeutic gene delivery systems.

1. Introduction

Development of safe and effective gene carriers is a key technology required for gene therapy. [1–5] A core issue for preparing non-viral gene carriers is the packaging of large pDNA molecules into the carrier system. Therefore, understanding the various packaging mechanisms is fundamental for the rational design and construction of gene carrier systems capable of achieving effective gene transfer. A key aspect of pDNA packaging is pDNA condensation. [6,7] DNA condensation is characterized as the large volume transition from a coil to a globule state, known as the coil–globule transition [8,9]. Until recently, the understanding of pDNA condensation has been mostly limited to morphological characterization of rod, toroid, and sphere structures [10,11] resulting from polyion complexation with polycations. Details pertaining to how and why pDNA is condensed into such structures and conditions required to selectively prepare these structures, as well as the effect of these packaging structure on gene expression remain to be fully clarified. This lack of understanding is mainly attributed to the difficulty of observing the condensation process of a single pDNA molecule, as condensation occurs concurrently with intercomplex aggregation particularly at charge-neutral ratios of polyions. To address this issue, block catiomers composed of a neutral hydrophilic poly(ethylene glycol) (PEG) segment and a cationic poly(L-lysine) (PLys) segment were used to induce controlled pDNA condensation into polymeric micelles, i.e., polyplex micelles. [12–15] In this approach pDNA is spontaneously condensed and packaged into a polyplex micelle core surrounded by PEG, eventually resulting in condensation of a single pDNA molecule without intercomplex aggregation. This allows for observation of the DNA condensation process even in the charge-neutral region. By using cationic block copolymers we have elucidated a highly regulated mechanism for pDNA condensation that involves folding into quantized-length rods. Rod lengths were found to be $1/2(n+1)$ of the original pDNA length by the folding of pDNA n times within polyplex micelles prepared with PEG-PLys 12–17 at the stoichiometric charge ratio (12 denotes the M_w of

* Corresponding author. Department of Materials Engineering, Graduate School of Engineering, The University of Tokyo, 7-3-1 Hongo, Bunkyo-ku, Tokyo 113-8656, Japan. Tel.: +81 3 5841 7138; fax: +81 3 5841 7139.
E-mail address: kataoka@bmw.t.u-tokyo.ac.jp (K. Kataoka).

0142-9612/$ – see front matter © 2011 Elsevier Ltd. All rights reserved.
doi:10.1016/j.biomaterials.2011.09.046

PEG in kDa, and 17 denotes Lys repeating units). [16] Furthermore, significantly higher gene expression efficiency was found in a cell-free transcription/translation system for pDNA packaged through the quantized folding within micelles compared to naked pDNA. Extension of this enhanced gene expression inherent to folded pDNA to living cells and ultimately whole organisms could greatly improve potential for therapeutic applications.

In this work, pDNA packaging within both rod and sphere shaped polyplex micelles was investigated, with a focus on DNA rigidity and folding. Selective preparation of rod or spherical structures was accomplished by modulating the PLys segment length of the block cationer. Moreover, the correlation of these packaging structures to gene expression efficiency was determined both *in vitro* and *in vivo*, with improved gene expression resulting from folded pDNA demonstrated in cultured cells as well as in skeletal muscle following intravenous (IV) injection.

2. Materials and methods

2.1. Materials

A series of poly(ethylene glycol)-*b*-poly(L-lysine) (PEG-PLys) block copolymers with different PLys segment lengths were synthesized via ring-opening polymerization of N^{ε}–trifluoroacetyl-L-lysine *N*-carboxyanhydride initiated by the ω–NH_2 terminal group of α–methoxy-ω-amino PEG (M_w 12 k), followed by removal of trifluoroacetyl groups (TFA) by NaOH. The degree of polymerization (DP) of PLys segments were determined to be 20, 34, 38, 51, 70, and 88, respectively by comparing ^{1}H NMR integration ratios between PEG chain methylene protons (CH_2CH_2O) and of lysine unit methylene protons ($(CH_2)_3CH_2NH_3$). PEG-PLys block copolymers with various PLys chain lengths were denoted as 12–20, 12–34, 12–38, 12–51, 12–70, and 12–88, respectively. Gel permeation chromatography (GPC) measurements were carried out using a TOSOH HLC-8220. Molecular weight distributions (M_w/M_n) for all these block copolymers were determined to be less than 1.1.

Packaging studies primarily utilized pBR322 (4361 bp) pDNA, luciferase T7 control DNA (4315 bp) was used for cell-free transcription/translation assays, and EGFP encoding pDNA was used for cytoplasmic injection. pGL4-Luc was used for *in vivo* gene transfer studies. These pDNAs were amplified in competent DH5α *Escherichia coli* and then purified using a HiSpeed Plasmid MaxiKit purchased from QUIAGEN Science Co. Inc. (Germany). Texas Red labeled-dextran (M_w 70,000) was purchased from Molecular Probes (USA).

2.2. Methods

2.2.1. Formation of pDNA/PEG-PLys polyplex micelles

PEG-PLys block copolymer and pDNA were separately dissolved in 10 mM Tris–HCl buffer adjusted to pH 7.4. Polyion complexes between PEG-PLys and pDNA (polyplex micelles) were obtained by simply mixing both solutions at stoichiometric charge ratio of lysine units in PEG-PLys to nucleotide units in pDNA (N/P ratio = 1). The final pDNA concentration of the complexes was adjusted to 33.3 μg/ml.

2.2.2. AFM imaging

Atomic force microscopy (AFM) imaging was conducted using an MMAFM, Nanoscope IIIa (Veeco, USA) in tapping mode with standard silicon probes on a highly orientated pyrolytic graphite (HOPG) substrate. The obtained images were processed by flattening to remove the background slope of the substrate surface.

2.2.3. TEM observation

TEM observation was conducted using an H-7000 electron microscope (Hitachi, Tokyo, Japan) operated at 75 kV acceleration voltage. Copper TEM grids with carbon-coated collodion film were glow-discharged for 20 s using an Eiko IB-3 ion coater (Eiko Engineering Co. Ltd., Japan). The grids were dipped into complex solution, which was mixed with uranyl acetate (UA) solution (2% (w/v)), for 30 s. After excess solution was removed using a filter paper, the sample grids were allowed to dry in air.

2.2.4. S1 nuclease digestion

S1 nuclease digestion of complexes was carried out in 30 mM sodium acetate buffer (pH 4.6) containing 1 mM $ZnSO_4$ for 30 min at 37 °C. The nuclease concentration was 5 units relative to 1 μg of pDNA. The reaction was stopped by the addition of excess ethylenediamine tetraacetic acid (EDTA). Ten equivalents (relative to nucleotides) of sodium dextran sulfate (M_w 25,000) was added to the solution for 1 h to dissociate the complex, followed by gel electrophoresis to determine the fragment lengths through a 0.9% agarose gel in electrophoresis buffer (20 mM Tris-AcOH, 10 mM NaOAc, 0.5 mM EDTA, and pH 7.8).

2.2.5. Cell-free transcription/translation assay

Cell-free gene expression efficiency was evaluated using the TnT Quick Coupled Transcription/Translation System (Promega Co., USA) using luciferase T7 control DNA coding the luciferase gene. Luciferase expression was achieved by mixing solutions of naked pDNA or polyplex micelles, each containing 1.33 μg of pDNA, with the solution from the cell-free system (TnT T7 Quick Master Mix) and this mixture was incubated for 90 min at 37 °C according to the protocol provided by the manufacturer. Luciferase expression was evaluated following addition of luciferase substrate (Luciferase Assay Reagent, Promega Co., USA) using a Mithras LB 940 luminometer (Berthold Technologies, Germany).

2.2.6. DNase I activity towards complexed pDNA

Solution containing DNase I (0.01 units, 25 mM $MgCl_2$ in Tris–HCl buffer (pH 7.4)) was added to the complex solution (pBR322, 33.3 μg/ml) and incubated at 37 °C. After the intended time, an excess amount of EDTA was added to stop the enzymatic reaction. Next, an excess amount of dextran sulfate was added to dissociate the polyplex micelles. After 3 h of incubation the solution was subjected to gel electrophoresis. DNA bands corresponding to supercoiled (SC), open-circular (OC), and linear forms were taken as the remaining pDNA, as these forms contribute to the transcription. DNase activity towards pDNA was determined by the intensity sum of the SC, OC, and linear forms respect to the intensity of non-DNase treated bands (naked pDNA) using densitometry.

2.2.7. In vitro transcription efficiency

A solution containing all necessary elements for transcription, *i.e.*, 0.5 mM ribonucleotides mixture (ATP, CTP, GTP, and UTP (Promega Co., USA)), 5 mM $MgCl_2$, 100 mM NaCl, and 5 mM DTT in10 mM Tris–HCl (pH 7.4) was added to solution containing either naked pDNA or pDNA complexed with PEG-PLys. T7 RNA polymerase (Promega Co., USA) (30 units) was then added to this mixture, followed by further incubation for 2 h at 37 °C. The solution was then incubated at 95 °C for 10 min to deactivate RNA polymerase. Template pDNA was digested by 30 units of DNase I at 37 °C for 2 h. PEG-PLys was digested by adding trypsin-EDTA at 37 °C for 2 h. Next, the solution was mixed with Quant-iT RiboGreen RNA reagent (fluorescent dye for RNA quantitation) for 30 min in the dark. Quantification of transcribed mRNA was determined using a spectro-fluorometer (λ_{ex} = 365 nm, λ_{em} = 590 nm). The fluorescence intensity of the transcribed mRNA from the polyplex micelles was normalized to that of mRNA from the naked pDNA.

2.2.8. Cytoplasmic microinjection

pDNA encoding for EGFP was injected into the cytoplasm of Huh-7 cells (100 cells) either in the naked form or packaged within polyplex micelles using a Micromanipulator NI2 and Microinjector FemtoJet (Eppendorf, Germany). Injections were conducted using depth limitation, with the settings of P_i = 100 hPa, P_c = 30 hPa and 0.1 s injection time, via glass micropipettes. Texas Red-labeled dextran (M_w 70,000), a charge-neutral fluorescence dye, was co-injected to allow estimation of the total injection volume. After 24 h incubation at 37 °C, 5% CO_2, the fluorescence intensity of EGFP was measured by fluorescence microscopy. Gene expression was quantified using expressed EGFP fluorescence and Texas Red-dextran fluorescence as a standard with following equation:

$$\sum_{i=1}^{n}\left[\left(I_{green}-I_{back.green}\right)/t_{GFP}\right]/\sum_{i=1}^{n}\left[\left(I_{red}-I_{back.red}\right)/t_{Texas-red}\right] \quad (1)$$

Here, I_{green} = fluorescence intensity of EGFP, $I_{back\ green}$ = fluorescence intensity of the background at the detection wavelength, I_{red} = fluorescence intensity of Texas Red-dextran, $I_{back\ red}$ = fluorescence intensity of the background at the detection wavelength, t_{GFP} or $t_{Texas\text{-}Red}$ = exposure time for EGFP or Texas Red, respectively. The value determined by the above equation yields gene expression activity per injected pDNA molecule.

2.2.9. In vivo gene transfer within skeletal muscle tissue

A solution containing naked pDNA or polyplex micelles (300 μL, 50 μg of luciferase-expressing pDNA) was injected into a distal site in the great saphenous vein of the mouse hind limb. A tourniquet was placed on the proximal thigh to transiently restrict blood flow prior to injection and remained in place until 5 min post-injection. Gene expression was determined 5 days post-injection by measuring bioluminescence with an IVIS™ Imaging System (Xenogen, USA). Images and measurements of bioluminescent signals were acquired and analyzed using Living Image software (Xenogen, USA). Ten minutes prior to *in vivo* imaging, the mice received the substrate D-luciferin (Biosynth, USA) at 150 mg/kg in PBS by intraperitoneal injection and were anesthetized using 1–3% isoflurane (Abbott Laboratories, USA). Animals were placed onto warmed (37 °C) stage inside the camera box and received continuous exposure to 1–2% isoflurane to sustain sedation during imaging. Luciferase expression was digitized and electronically displayed as a pseudocolor overlay onto a gray scale animal image. All animal experimental procedures were performed in accordance with the Guide for the Care and Use of Laboratory Animals as stated by the University of Tokyo.

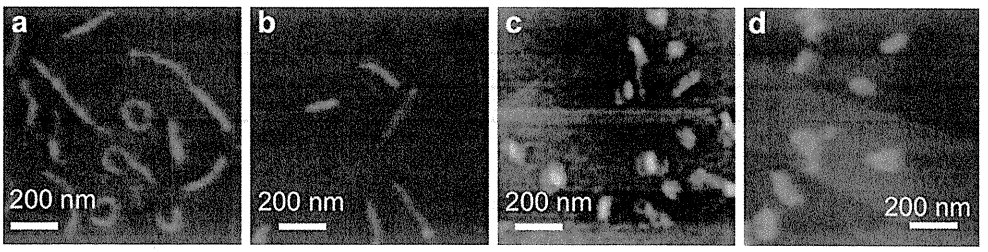

Fig. 1. AFM images of polyplex micelles. (a) 12–20, (b) 12–38, (c) 12–51, and (d) 12–70. All images were acquired in tapping mode.

3. Results and discussion

3.1. Packaging of pDNA within polyplex micelles

In order to further explore the packaging of pDNA within polyplex micelles, the structures of 12–20, 12–38, 12–51, and 12–70 polyplex micelles prepared at charge stoichiometric ratio were investigated using atomic force microscopy (AFM). Rod and toroid structures were observed for 12–20 and 12–38 polyplex micelles (Fig. 1a and b), similar to previously studied 12–17 based polyplex micelles. Careful analysis of 12–17 polyplex micelles revealed that rod structures formed as a result of the quantized folding of pDNA. [16] In contrast, spherical structures were obtained for 12–51 and 12–70 polyplex micelles (Fig. 1c and d). In the case of 12–20 and 12–38 polyplex micelles, precise rod lengths were measured from TEM images (representative TEM images are shown in Supporting Information 1) to determine whether or not rod structures follow the quantized folding model. It should be noted that TEM was performed with uranyl acetate (UA) staining, which allows selective observation of DNA due to the stronger affinity of UA to DNA compared to PEG. According to the quantized folding model (Fig. 2a), rod lengths are restricted to 1, 1/2, 1/3, 1/4 increments relative to the length of an unfolded rod structure (depicted in Fig. 2a structure (i)). Using the unfolded rod structure as a standard, which is calculated to be 611 nm for pBR322 (4361 bp) [16], the theoretical rod lengths are calculated to be 305, 203, 152, 122, 102, 87, and 76 nm by folding of pDNA 1, 2, 3, 4, 5, 6, and 7 times, respectively (Table 1). Note that estimation of the standard rod length (611 nm) involves, (1) simply collapsing the circular DNA results in half of the contour length (4361 (bp) × 0.338 (nm/bp)/2), (2) length reduction due to the coiled-coil form of pDNA caused by its inherent superhelicity, and (3) artifacts in TEM observation on a collodion substrate with UA staining [17]. These theoretical rod lengths (shown as dotted lines in Fig. 2b) correlate very well to

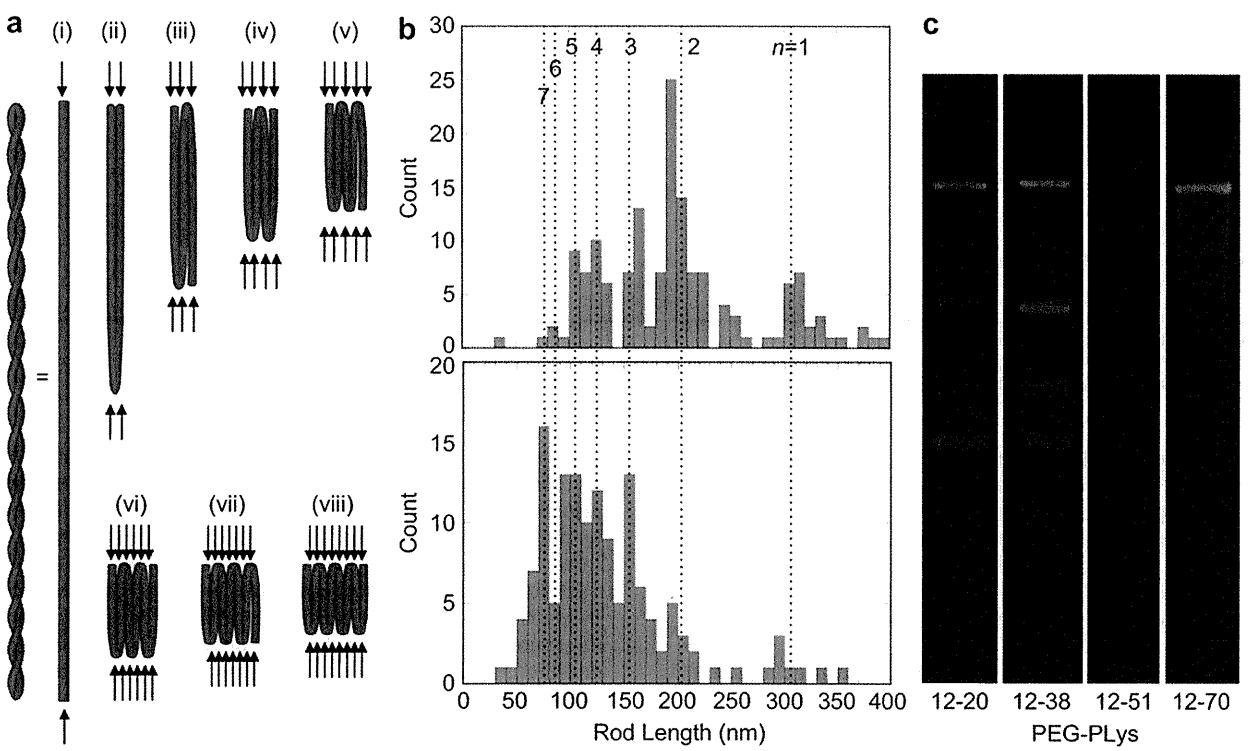

Fig. 2. Quantized folding of pDNA into polyplex micelles. (a) Schematic illustration of pDNA condensation into rod structures with quantized folding. The rod structure formed by simply collapsing supercoiled circular pDNA is depicted as (i). For simplification, intertwining due to superhelicity is not pictured. S1 nuclease-susceptible sites (sites of single-stranded DNA formed by dissociation of double-stranded DNA) are indicated by arrows. Note that the PEG shell is not pictured and that folded DNA strands are depicted in 2-dimentions for simplicity, however they are 3-dimensionally packed into bundles. (b) Distribution of the long axis length of the rod structures measured from TEM images for the polyplex micelles of 12–20 (top, 168 counts) and 12–38 (bottom, 141 counts). Dotted lines represent calculated rod lengths according to quantized folding. (c) S1 nuclease activity toward the polyplex micelles of 12–20, 12–38, 12–51 and 12-70 determined by gel electrophoresis.

Table 1
Expected fragment fractions and length of the rod structures in the quantized folding model.

Expected fregment fraction[a]								Fraction	Fragment No. in Table 2
$n = 0$	$n = 1$	$n = 2$	$n = 3$	$n = 4$	$n = 5$	$n = 6$	$n = 7$		
2/2	4/4	6/6	8/8	10/10	12/12	14/14	16/16	1.00	1
							15/16	0.94	
						13/14		0.93	
					11/12			0.92	
				9/10				0.90	
			7/8				14/16	0.88	
						12/14		0.86	
		5/6			10/12			0.83	2
							13/16	0.81	
				8/10				0.80	
						11/14		0.79	
	3/4		6/8		9/12		12/16	0.75	3
						10/14		0.71	
				7/10				0.70	
							11/16	0.69	
		4/6			8/12			0.67	4
						9/14		0.64	
			5/8				10/16	0.63	
				6/10				0.60	
					7/12			0.58	(5)[c]
						8/14		0.57	5
							9/16	0.56	(5)
1/2	2/4	3/6	4/8	5/10	6/12	7/14	8/16	0.50	6
							7/16	0.44	
						6/14		0.43	(7)
					5/12			0.42	7
				4/10				0.40	
			3/8				6/16	0.38	8
						5/14		0.36	
		2/6			4/12			0.33	9
							5/16	0.31	
				3/10				0.30	
						4/14		0.29	10
	1/4		2/8		3/12		4/16	0.25	11
						3/14		0.21	
				2/10				0.20	12
							3/16	0.19	(12)
		1/6			2/12			0.17	13
						2/14		0.14	14
			1/8				2/16	0.13	15
				1/10				0.10	
					1/12			0.08	
						1/14		0.07	
							1/16	0.06	
multiples and expected length[b] (nm)									
x/2	x/4	x/6	x/8	x/10	x/12	x/14	x/16		
611	306	204	153	122	102	87	76		

[a] Ratio respect to the original pDNA length.
[b] Expected rod length in TEM images considering shrinkages due to the supercoiling and use of collodion substrate with UA staining.
[c] Fragment number in brackets is candidate for the band in Table 2.

measured rod length distributions from TEM images, suggesting that the rod structures of 12–20 and 12–38 polyplex micelles were formed by quantized folding. As seen in Fig. 2b, the rod size distribution of 12–38 polyplex micelles was found to be shorter compared to 12–20 polyplex micelles. Note that no rod structures were observed for 12–51 and 12–70 polyplex micelles (Fig. 1c and d), thus rod length distribution was not measured.

3.2. Integrity of double-stranded DNA within polyplex micelles

We previously reported that rod structures are formed by folding rigid double-stranded DNA (persistence length (l_p) of approximately 50 nm [18]) at the rod ends via hairpin turns. This is made possible by dissociation of the double-stranded structure into more flexible single-strand species [19] with l_p of only a few nanometers [20] or less. [21] Double-strand dissociation sites, or fold sites, were detected by S1 nuclease digestion, as this nuclease is a single-strand specific cleavage enzyme. Enzymatic digestion revealed a characteristic fragmentation pattern with lengths corresponding to multiples of $1/2(n + 1)$ of the original pDNA length, with n being the folding number (expected fragments are listed in Table 1). Thus, polyplex micelles were subjected to S1 nuclease digestion in this study to investigate the integrity of double-stranded DNA contained within the polyplex micelles. A distinct fragmentation pattern was obtained for 12–20 and 12–38 polyplex micelles (Fig. 2c). Analysis of fragments showed that the ratios of fragment length with respect to the original pDNA length (Table 2) corroborated well with expected fragment lengths (Table 1) assuming quantized folding of pDNA within 12–20 and 12–38 polyplex micelles. In contrast, the gel electrophoresis profiles for 12–51 and 12–70 polyplex micelles were smeared and faint (Fig. 2c). This suggests that dissociation and nuclease cleavage of the double-stranded DNA structure occurred randomly. Note that these polyplex micelles were observed to adopt irregular and

Table 2
Fragment lengths and fractions respect to the linearized pDNA length for pBR322 complexed by PEG-PLys block catiomers.

No.	Fragment length (bp)[a] and fractions[b]						Possible folding number
	PEG-PLys 12–20			PEG-PLys 12–38			
1	s[c]	4452	1	s	4458	1	0,1,2,3,4,5,6,7
2		3799	0.85	s	3712	0.83	2,5
3	s	3195	0.71	s	3328	0.75	1,3,5,7,
4	s	2943	0.66	s	2962	0.66	2,5
5		2555	0.57		2540	0.57	6 (or 5,7)[d]
6	s	2228	0.5	s	2223	0.5	0,1,2,3,4,5,6,7
7		1925	0.43		1885	0.42	5 (or 6)
8					1666	0.37	7
9		1482	0.33	s	1466	0.33	2,5
10		1263	0.28		1262	0.28	6 (or 4)
11	s	1063	0.24	s	1078	0.24	1,3,5,7
12		854	0.2		861	0.19	4 (or 7)
13		727	0.16	s	726	0.16	2,5
14		634	0.14				6
15					564	0.13	3,7

[a] Fragment length were estimated from size marker.
[b] Each fragment length was devided by the length of the linear band, *i.e.*, fragment no.1.
[c] s; band with strong fluorescence intensity.
[d] () possible folding number.

compact spherical structures in AFM images (Fig. 1c and d). Formation of such compact structures by the regular folding of rigid double-stranded DNA seems unlikely, considering the appreciably long l_p of ~50 nm for native double-stranded DNA [18] and the even longer l_p of ~90 nm for pDNA complexed with PEG-PLys (due to the formation of the intertwining coiled-coil structure). [16] Presumably, dissociation of the double-stranded DNA structure and exposure of S1 nuclease-susceptible single strands may occur randomly at many sites within these polyplex micelles, eventually leading to formation of collapsed structures as a result of flexible single-stranded DNA.

Both AFM and S1 nuclease digestion results suggest that there is a correlation between the micelle structure and the double-stranded structure of pDNA contained in the micelle core. It is likely that integrity of pDNA double-stranded structure, in other words rigidity of DNA, plays a crucial role in discriminating between packaging structures. DNA double-strand dissociation and subsequent folding or collapsing is influenced by the PLys segment length upon complexation with block catiomer. The critical PLys length that divides packaging structures into folded rods or collapsed spheres is located between 38 and 51 amino acid units. Studies devoted to providing further insight into the mechanisms involved in this critical phenomenon are currently underway in our lab, and results will be reported in the near future.

3.3. *Effect of pDNA packaging on in vitro gene expression*

As described in the preceding section, structures of polyplex micelles are modulated by the PLys segment length and are categorized into two groups; 1) quantized folding packaging (12–20 and 12–38 polyplex micelles) mediated by a highly regulated folding mechanism, and 2) collapsed packaging (12–51 and 12–70 polyplex micelles), possibly accompanied by random dissociation of double-stranded DNA structure. Here, we addressed the relationship between the structure of the polyplex micelles and their transfection efficiency. Although polyplex micelles were prepared in solution without NaCl for characterization studies in the preceding section, the obtained results are reasonably extended to physiological buffer conditions used in biological assays because there was no substantial difference in the size and shape between polyplex micelles prepared at 0 and 150 mM NaCl judging from dynamic light scattering (DLS) measurement and TEM observation (Figs. S1 and S2 of the Supporting Information).

We have previously reported that polyplex micelles containing quantized folded pDNA, prepared from PEG-PLys 12–17, exhibit higher gene expression efficiency than naked pDNA in the cell-free transcription/translation assay system for luciferase expression. [16] This motivated us to compare the gene transfection efficiency of pDNA contained in micelles with different packaging modes depending on PLys length of the block copolymer. As seen in Fig. 3a, regularly folded pDNA contained in the core of polyplex micelles prepared with 12–20 and 12–38 achieved significantly higher luciferase expression than naked pDNA in the cell-free system reconstructed from rabbit reticulocyte cell lysate. This is consistent with our previous results obtained for polyplex micelles prepared with 12–17, which also comprise regularly folded pDNA [16]. Luciferase expression decreased for the collapsed pDNA in 12–70 polyplex micelles compared to the regularly folded pDNA in 12–20 and 12–38 polyplex micelles. Naked pDNA had the lowest expression efficiency out of all the formulations tested, even lower than 12–70 polyplex micelles, but this is likely due to poor tolerability of naked pDNA against nuclease degradation in the cell lysate [16]. Indeed, increased resistance against DNase I degradation was confirmed for all of the polyplex micelles regardless of the packaging mode, whereas naked pDNA was promptly digested under the same conditions (Fig. 3b).

Then, transcription efficiency of pDNA in different packaging modes was examined separately from the translation process, in conditions without interference from lysate components including nuclease. In this experiment, a reconstructed solution containing all necessary transcription components, i.e., ribonucleotides and RNA polymerases, was used, and the results are shown in Fig. 3c. No appreciable difference in transcription activity between 12–20 and 12–38 polyplex micelles and naked pDNA was observed, which is consistent with the view that decreased gene expression efficiency of native pDNA in cell-free system was caused by nuclease degradation (Fig. 3a). Collapsed pDNA contained in 12–70 polyplex micelles showed significantly lower transcription activity than the regularly folded pDNA contained in 12–20 and 12–38 micelles. This corroborates well with the trend observed in the gene expression assay shown in Fig. 3a, and suggests that a difference in transcription activity between regularly folded and randomly collapsed pDNA ultimately determines the final efficiency of gene expression.

Transcription requires that transcription machinery must first access, and then slide along double-stranded DNA. Comparable transcription activity of native pDNA with regularly folded pDNA contained in 12–20 and 12–38 polyplex micelles suggests that these transcription processes may not be hindered by the block copolymers complexed with pDNA. Presumably, exchange of these block copolymers with transcription machinery may occur in the transcription processes for regularly folded pDNA with a well-preserved double-stranded structure. Another possibility is that polyplexes already dissociated in solution prior to transcription, but that is apparently not the case. As seen in Fig. 3b, pDNA in the 12–20 and 12–38 polyplex micelles showed appreciably higher resistance against nuclease digestion than native pDNA, indicating the polyplex stability in medium. Alternatively, the significantly lowered transcription activity of collapsed pDNA contained in 12–70 polyplex micelles indicates that transcription machinery is substantially impeded in this case. It is of interest to note that the S1 nuclease digestion study (Fig. 2c) demonstrated substantial and random disruption of the double-stranded DNA structure packaged in the 12–70 polyplex micelle. Thus, one plausible reason for transcription inhibition may be the inability of transcription machinery to slide along DNA strands. However, decreased

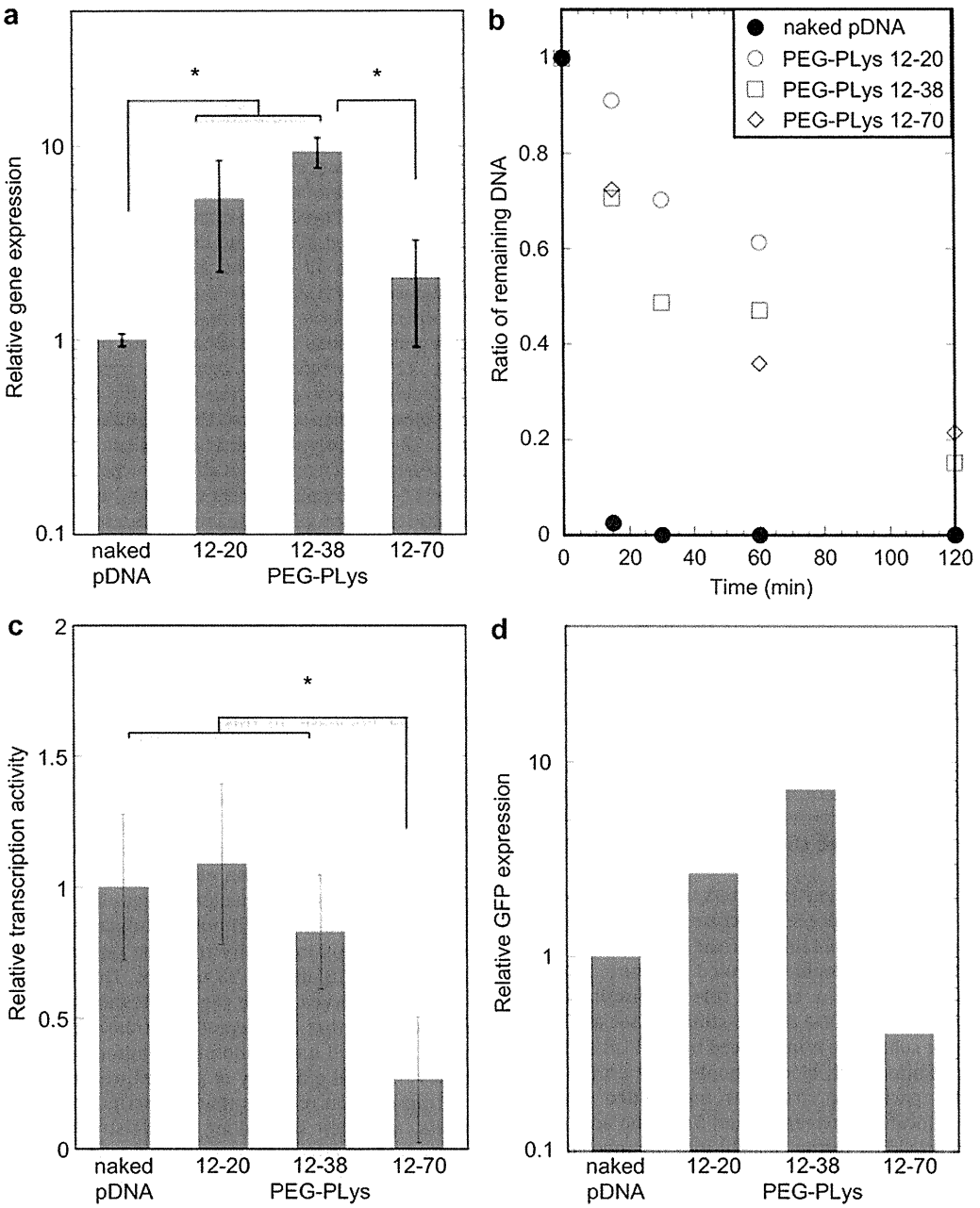

Fig. 3. Biological evaluation of polyplex micelles containing pDNA in different packaging modes. PEG-PLys 12–20 and 12–38 micelles represent folded rod structures whereas 12–70 micelles represent collapsed sphere structures. (a) Gene expression efficiency in the cell-free transcription/translation assay system. Relative light units (RLU) of luciferase expression were normalized to naked pDNA. ($n = 6$, Mean ± SD, $P^* < 0.05$). (b) DNase I degradation as a function of incubation time. (c) *In vitro* transcription efficiency evaluated in a solution containing all elements needed for transcription. The amount of transcribed RNA was normalized to naked pDNA. ($n = 4$, Mean ± SD, $p^* < 0.05$). (d) Gene expression efficiency after cytoplasmic microinjection of naked pDNA and polyplex micelles into Huh-7 cells (100 cells). EGFP gene expression from the polyplex micelles was normalized against that of naked pDNA.

transcription might also be explained simply by the increased DNA binding affinity of the longer cationic PLys segment in 12–70 compared to 12–20 and 12–38, preventing binding and movement of transcription machinery along DNA strands.

Demonstration of improved gene expression in living cells due to the folded packaging of pDNA within polyplex micelles could have significant impacts on therapeutic applications. To examine this possibility, pDNA encoding for EGFP was injected directly into the cytosol of Huh-7-cells either in the naked form or contained in polyplex micelles. As seen in Fig. 3d, enhanced gene expression for 12–20 and 12–38 polyplex micelles compared to naked pDNA was observed, whereas 12–70 polyplex micelles resulted in the lowest expression. This trend correlates well with results obtained in the cell lysate study as shown in Fig. 3a, confirming improved gene expression in the living cell system due to the folded packaging of pDNA. The substantial decrease in gene expression for naked pDNA may be due to nuclease attack and degradation in the cytosol. [22] It is therefore noteworthy to address that enhanced gene

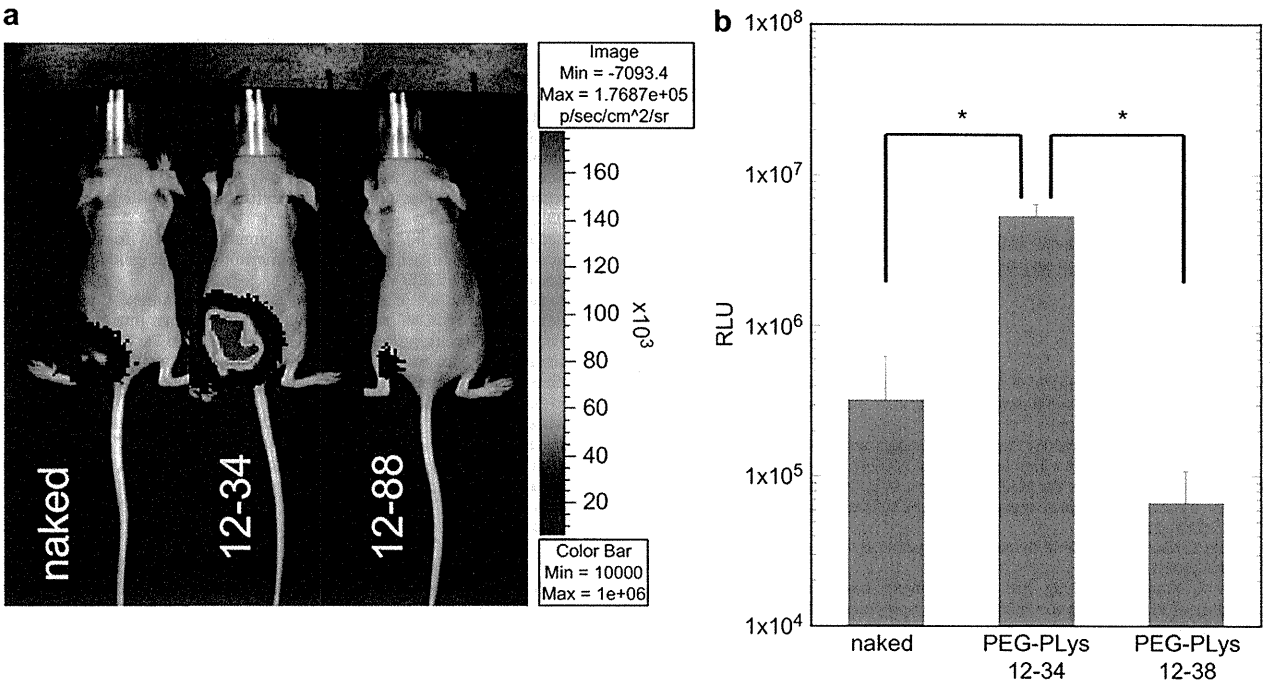

Fig. 4. *In vivo* gene transfer in skeletal muscle following IV injection of naked pDNA or corresponding polyplex micelles during tourniquet application. (a) IVIS images and (b) quantified results ($n = 6$, Mean ± SD. $P^* < 0.05$).

expression demonstrated by folded pDNA packaging may be attributed to its nuclease-tolerability and transcription-active nature.

3.4. *Effect of pDNA packaging on in vivo gene expression*

Enhanced gene expression due to the folded packaging of pDNA demonstrated in these *in vitro* evaluations motivated us to extend this system to an *in vivo* application. Recently, efficient and safe gene transfer of naked pDNA targeted to skeletal muscle tissue via IV injection in conjunction with a tourniquet was reported. [23,24] Using this method, naked pDNA encoding for luciferase and corresponding polyplex micelles of 12–34 and 12–88, representing folded and collapsed pDNA packaging respectively, were injected into the great saphenous vein of the distal hind limb during temporal tourniquet application. Luciferase expression within skeletal muscle was evaluated by measuring luminescence with an *in vivo* imaging system (IVIS) (Fig. 4). Naked pDNA exhibited significant luciferase expression, which is consistent with the previous report. [23] Gene expression for 12–34 polyplex micelles was much higher than that of naked pDNA, suggesting that enhanced gene expression due to folded packaging occurs even *in vivo*. Significantly lower gene expression was observed for 12–88 polyplex micelles, indicating that controlled packaging of pDNA is critically important for effective gene expression. Targeted gene expression within skeletal muscle is attractive in a practical sense, not only for direct treatment of the diseases in the muscle such as muscular dystrophy, but also as a "protein factory" expressing transgenes continuously and distributing the protein products to the whole body [24–26].

We have previously reported safe and sustained transgene expression in skeletal muscle using the same administration technique used here, and obtained significant tumor growth suppression through the anti-angiogenic effect of the soluble vascular endothelial growth factor (VEGF) receptor-1 (sFlt-1) gene. [24] In that study, 12–16 and 12–38 polyplex micelles exhibited higher gene expression than that of 12–88 polyplex micelles and naked pDNA. This result can now be reasonably understood as the effect of folded pDNA packaging, and concurrently highlights the potential of this packaging formulation for practical therapeutic applications.

4. Conclusions

pDNA packaging within the polyplex micelles was significantly affected by PLys segment length in PEG-PLys block catiomers and two distinct packaging modes were demonstrated, namely, folded packaging through quantized folding and collapsed packaging accompanied by substantial disruption of the double-stranded DNA structure. Higher gene expression resulting from folded pDNA packaging compared to collapsed packaging and naked pDNA was shown not only in a cell-free system and in living cells by cytoplasmic microinjection, but also *in vivo* within skeletal muscle following IV injection. Enhanced gene expression demonstrated by folded pDNA packaging may be attributed to its nuclease-tolerability and transcription-active nature. Results obtained for regularly folded pDNA polyplex micelles were in stark contrast with collapsed pDNA polyplex micelles, probably due to limited transcription efficiency, clearly showing that controlled packaging of pDNA is crucial for achieving effective gene transfer. Promotion of gene transfer through controlled folded packaging of pDNA demonstrates the potential for application of this polyplex micelle system for practical use.

Acknowledgments

This work was financially supported by the Core Research Program for Evolutional Science and Technology (CREST) from the Japan Science and Technology Corporation (JST), by the Japan Society for the Promotion of Science (JSPS) through its "Funding

Program for World-Leading Innovative R&D on Science and Technology (FIRST Program)" and by the Center for Medical System Innovation (CMSI) (Global COE Program, MEXT). The authors also thank Mr. Matthew Pennisi for assistance with manuscript preparation.

Appendix. Supplementary material

Supplementary data associated with this article can be found, in the online version, at doi:10.1016/j.biomaterials.2011.09.046

References

[1] Kataoka K, Harada A, Nagasaki Y. Block copolymer micelles for drug delivery: design, characterization and biological significance. Adv Drug Deliv Rev 2001; 47:113–31.
[2] Pack DW, Hoffman AS, Pun S, Stayton PS. Design and development of polymers for gene delivery. Nat Rev Drug Discov 2005;4:581–93.
[3] Mastrobattista E, van der Aa MAEM, Hennink WE, Crommelin DJA. Artificial viruses: a nanotechnological approach to gene delivery. Nat Rev Drug Discov 2006;5:115–21.
[4] Wagner E, Kloeckner J. Gene delivery using polymer therapeutics. Adv Polym Sci 2006;192:135–73.
[5] Osada K, Kataoka K. Drug and gene delivery based on supramolecular assembly of PEG-polypeptide hybrid block copolymers. Adv Polym Sci 2006; 202:113–53.
[6] Laemmli UK. Characterization of DNA condensates induced by poly(ethylene oxide) and polylysine. P Natl Acad Sci USA 1975;72:4288–92.
[7] Bloomfield VA. DNA condensation. Curr Opin Struct Biol 1996;6:334–41.
[8] Stockmayer WH. Problems of the statistical thermodynamics of dilute polymer solutions. Makromol Chem 1960;35:54–74.
[9] Melnikov SM, Sergeyev VG, Yoshikawa K. Discrete coil-globule transition of large DNA induced by cationic surfactant. J Am Chem Soc 1995;117:2401–8.
[10] Eickbush TH, Moudrianakis EN. Compaction of DNA helices into either continuous supercoils or folded-fiber rods and toroids. Cell 1978;13:295–306.
[11] Kwoh DY, Coffin CC, Lollo CP, Jovenal J, Banaszczyk MG, Mullen P, et al. Stabilization of poly-L-lysine/DNA polyplexes for *in vivo* gene delivery to the liver. Biochim Biophys Acta 1999;1444:171–90.
[12] Katayose S, Kataoka K. Water-soluble polyion complex associates of DNA and poly(ethylene glycol)-poly(L-lysine) block copolymer. Bioconjug Chem 1997; 8:702–7.
[13] Kakizawa Y, Harada A, Kataoka K. Environment-sensitive stabilization of core-shell structured polyion complex micelle by reversible cross-linking of the core through disulfide bond. J Am Chem Soc 1999;121:11247–8.
[14] Itaka K, Yamauchi K, Harada A, Nakamura K, Kawaguchi H, Kataoka K. Polyion complex micelles from plasmid DNA and poly(ethylene glycol)-poly(L-lysine) block copolymer as serum-tolerable polyplex system: physicochemical properties of micelles relevant to gene transfection efficiency. Biomaterials 2003;24:4495–506.
[15] Osada K, Christie RJ, Kataoka K. Polymeric micelles from poly(ethylene glycol)-poly(amino acid) block copolymer for drug and gene delivery. J R Soc Interface 2009;6:S325–39.
[16] Osada K, Oshima H, Kobayashi D, Doi M, Enoki M, Yamasaki Y, et al. Quantized folding of plasmid DNA condensed with block catiomer into characteristic rod structures promoting transgene efficacy. J Am Chem Soc 2010;132:12343–8.
[17] Namork E, Johansen BV. Electron-microscopy of nucleic-acids - effect of different post-treatments on contour-length measurements. Micron 1980;11: 85–90.
[18] Eisenberg H. DNA flexing, folding, and function. Acc Chem Res 1987;20: 276–82.
[19] Osada K, Yamasaki Y, Katayose S, Kataoka K. A synthetic block copolymer regulates S1 nuclease fragmentation of supercoiled plasmid DNA. Angew Chem Int Edit 2005;44:3544–8.
[20] Tinland B, Pluen A, Sturm J, Weill G. Persistence length of single-stranded DNA. Macromolecules 1997;30:5763–5.
[21] Smith SB, Cui YJ, Bustamante C. Overstretching B-DNA: the elastic response of individual double-stranded and single-stranded DNA molecules. Science 1996;271:795–9.
[22] Glasspool-Malone J, Steenland PR, McDonald RJ, Sanchez RA, Watts TL, Zabner J, et al. DNA transfection of macaque and murine respiratory tissue is greatly enhanced by use of a nuclease inhibitor. J Gene Med 2002;4:323–32.
[23] Hagstrom JE, Hegge J, Zhang G, Noble M, Budker V, Lewis DL, et al. A facile nonviral method for delivering genes and siRNAs to skeletal muscle of mammalian limbs. Mol Ther 2004;10:386–98.
[24] Itaka K, Osada K, Morii K, Kim P, Yun SH, Kataoka K. Polyplex nanomicelle promotes hydrodynamic gene introduction to skeletal muscle. J Control Release 2010;143:112–9.
[25] Blau HM, Springer ML. Muscle-mediated gene therapy. N Engl J Med 1995; 333:1554–6.
[26] Lu QL, Bou-Gharios G, Partridge TA. Non-viral gene delivery in skeletal muscle: a protein factory. Gene Ther 2003;10:131–42.

Journal of Controlled Release 155 (2011) 296–302

Contents lists available at ScienceDirect

Journal of Controlled Release

journal homepage: www.elsevier.com/locate/jconrel

Combination of chondroitin sulfate and polyplex micelles from Poly(ethylene glycol)-poly{N'-[N-(2-aminoethyl)-2-aminoethyl]aspartamide} block copolymer for prolonged in vivo gene transfection with reduced toxicity

Satoshi Uchida [a], Keiji Itaka [a,*], Qixian Chen [b], Kensuke Osada [b], Kanjiro Miyata [a], Takehiko Ishii [c], Mariko Harada-Shiba [d], Kazunori Kataoka [a,b,**]

[a] Division of Clinical Biotechnology, Center for Disease Biology and Integrative Medicine, Graduate School of Medicine, The University of Tokyo, 7-3-1 Hongo, Bunkyo-ku, Tokyo, Japan 113-0033
[b] Department of Materials Science and Engineering, Graduate School of Engineering, The University of Tokyo, 7-3-1 Hongo, Bunkyo-ku, Tokyo, Japan 113-0033
[c] Department of Bioengineering, Graduate School of Engineering, The University of Tokyo, 7-3-1 Hongo, Bunkyo-ku, Tokyo, Japan 113-0033
[d] Department of Molecular Pharmacology, National Cerebral and Cardiovascular Center Research Institute, 5-7-1 Fujishiro-dai, Suita, Osaka, Japan 565-8565

ARTICLE INFO

Article history:
Received 7 March 2011
Accepted 27 April 2011
Available online 5 May 2011

Keywords:
Polyplex micelle
Chondroitin sulfate
Gene delivery
Block catiomer
Membrane toxicity

ABSTRACT

Nonviral polycation-based gene carriers (polyplexes) have attracted attention as safe and efficient gene delivery systems. Polyplex micelles comprised of poly(ethyleneglycol)-*block*-poly{N'-[N-(2-aminoethyl)-2-aminoethyl]aspartamide} (PEG-PAsp(DET)) and plasmid DNA (pDNA) have shown high transfection efficiency with low toxicity due to the pH-sensitive protonation behavior of PAsp(DET), which enhances endosomal escape, and their self-catalytic degradability under physiological conditions, which reduces cumulative toxicity during transfection. In this study, we improved the safety and transfection efficiency of this polyplex micelle system by adding an anionic polycarbohydrate, chondroitin sulfate (CS). A quantitative assay for cell membrane integrity using image analysis software showed that the addition of CS markedly reduced membrane damage caused by free polycations in the micelle solution. It also reduced tissue damage and subsequent inflammatory responses in the skeletal muscle and lungs of mice following *in vivo* gene delivery with the polyplex micelles. Subsequently, this led to prolonged transgene expression in the target organs. This combination of polyplex micelles and CS holds great promise for safe and efficient gene introduction in clinical settings.

1. Introduction

Gene therapy has been explored for treating numerous diseases, including genetic disorders and cancers. Cationic polymers are often used for constructing nonviral gene carriers termed polyplexes, due to their advantages, such as large DNA loading capacity, ease of large-scale production, and reduced immunogenicity that has been an issue associated with viral vectors [1–3]. However, an inherent problem with using cationic polymers for gene transfection is their toxicity that causes tissue damage. The positively charged nature of polyplexes can induce nonspecific interactions with anionic biological molecules, such as blood cells, serum proteins, and extracellular matrices, which hinder the efficient delivery of genes, especially for *in vivo* applications.

A promising strategy to resolve these issues is to incorporate a hydrophilic protective layer of poly(ethylene glycol) (PEG) on the surfaces of polyplexes. A polyplex micelle system originally developed by our group is a good example of PEGylated polyplexes. In this system, PEG-polycation block copolymers are complexed with plasmid DNA (pDNA) to form a micellar structure that has a surface with hydrophilic and electrically neutral PEG and an inner core containing pDNA in a condensed state [4–8]. This structure increases the steric stability of the polyplexes under physiological conditions and exhibits less nonspecific interactions with biological components, such as serum proteins. In addition, a new polycation, poly{N'-[N-(2-aminoethyl)-2-aminoethyl]aspartamide} (PAsp(DET)), used as a core-forming segment of polyplex micelles, was developed to increase transfection efficiency [6].

Comprehensive analyses revealed that the high gene transfection capability of PAsp(DET) was mainly attributed to two distinct properties: (1) pH-responsive change in the degree of protonation, which enhanced endosomal escape [9] and (2) self-catalytic degradability under physiological conditions, which reduced the cumulative toxicity during transfection [10]. Using PEG-PAsp(DET) block copolymers, we achieved effective and sustained transgene expressions for *in vivo* local administration [11] and succeeded in bone

* Correspondence to: K. Itaka, Division of Clinical Biotechnology, Center for Disease Biology and Integrative Medicine, Graduate School of Medicine, The University of Tokyo, 7-3-1 Hongo, Bunkyo-ku, Tokyo 113-0033, Japan. Tel.: +81 3 5841 1418; fax: +81 3 5841 1419.
** Correspondence to: K. Kataoka, Department of Materials Engineering, Graduate School of Engineering, The University of Tokyo, 7-3-1 Hongo, Bunkyo-ku, Tokyo 113-0033, Japan. Tel.: +81 3 5841 7138; fax: +81 3 5841 7139.
E-mail addresses: itaka-ort@umin.ac.jp (K. Itaka), kataoka@bmw.t.u-tokyo.ac.jp (K. Kataoka).

0168-3659/$ – see front matter © 2011 Elsevier B.V. All rights reserved.
doi:10.1016/j.jconrel.2011.04.026

regeneration by introducing osteogenic factor-expressing genes for bone defects in the mouse skull [8].

These PEG-PAsp(DET)/pDNA polyplex micelles (PMs) were applied to bone defect areas after their incorporation into a scaffold. Among several scaffolds tested, a commercial calcium phosphate paste (BIOPEX-R; Mitsubishi Pharma, Osaka, Japan) yielded the highest transgene expression. BIOPEX-R contains a considerable amount of chondroitin sulfate (CS), an anionic polycarbohydrate. This result led us to hypothesize that CS might play a critical role in gene introduction using PMs.

This study was designed to verify this hypothesis. We sought to identify the mechanisms involved with improved transfection after the addition of CS to PMs using physicochemical analyses, *in vitro* transfection, and *in vivo* local gene transfer.

2. Materials and methods

2.1. Materials

Plasmid DNA (pDNA) encoding luciferase (pGL4.13: Promega, Madison, WI) was amplified in competent DH5α *Escherichia coli* and purified using NucleoBond Xtra EF (Nippon Genetics, Tokyo, Japan). The pDNA concentration was determined from the absorbance at 260 nm. Dulbecco's modified Eagle's medium was from Sigma-Aldrich (St. Louis, MO, USA) and fetal bovine serum was from Dainippon Sumitomo Pharma Co., Ltd. (Osaka, Japan). Chondroitin sulfate A (CS) was from Sigma-Aldrich. Linear polyethyleneimine (LPEI) (Exgen 500; MW = 22 kDa) was from MBI Fermentas (Burlington, ON, Canada).

2.2. Animals

ICR mice (female, 7 weeks old) were purchased from Charles River Laboratories. All animal protocols were conducted with the approval of the Animal Care and Use Committee of the University of Tokyo.

2.3. Preparation of polyplex micelle solutions

PEG-PAsp(DET) block copolymer was synthesized as previously reported [6]. The PEG used had a molecular weight of 12,000 and the polymerization degree of the PAsp(DET) portion was determined to be 69 by ^{1}H-NMR. PEG-PAsp(DET) block copolymers and pDNA were separately dissolved in 10 mM Tris–HCl buffer (pH 7.4). PEG-PAsp (DET)/pDNA polyplex micelles (PMs) were obtained by simply mixing both solutions. After mixing for 10 min, PEG-PAsp(DET)/pDNA/CS polyplex micelles (CS-PMs) were prepared by adding CS at varying concentrations. In this study, the residual molar ratio of amino groups in PEG-PAsp(DET), phosphate groups in pDNA, and the total carboxyl and sulfate groups in CS was defined as N:P:CS. The final pDNA concentration was adjusted to 30 μg/ml for *in vitro* experiments and 133 μg/ml for *in vivo* experiments.

2.4. Luciferase expression and cell viability after transfection of PMs and CS-PMs

Cells were seeded at a density of 5000 cells/well in a 96-multiwell plate and cultured for 24 h. After the culture medium was replaced with fresh medium containing 10% fetal bovine serum, PMs or CS-PMs containing 0.18 μg pDNA was added to each well. Firefly luciferase expression was determined using a Luciferase assay system (Promega, Madison, WI, USA) and a GloMaxTM 96 microplate luminometer (Promega) following the manufacturer's protocol. Cell viability was determined using a Cell Counting Kit-8 (Dojindo, Kumamoto, Japan) following the manufacturer's protocol.

2.5. Quantitative assay for the cellular uptake of pDNA

Cells were seeded at a density of 80,000 cells/well in a 6-multiwell plate and transfection was performed as in the previous section using 4 μg pDNA/well. Plasmid DNA was collected and purified from each well using a Wizard Genomic DNA purification kit (Promega). Purified DNA was then subjected to real time polymerase chain reaction (PCR) for the quantification of pDNA copies encoding Luc2 using an ABI Prism 7500 Sequence Detector (Applied Biosystems, Foster City, CA) and the following primers: forward primer GGACTTGGACACCGG-TAAGA and reverse primer GTCGAAGATGTTGGGGTGTT. The copy number of β-actin was also determined by TaqMan Gene Expression Assays (Applied Biosystems) to normalize the cell number.

2.6. Evaluation of cell membrane integrity

Cells were seeded at a density of 10,000 cells/well in a 48-multiwell plate and cultured for 24 h. After the culture medium was replaced with PBS, PMs or CS-PMs containing 0.5 μg pDNA was added to each well. The cells were treated with 1 μM YO-PRO1 and 2.5 μg/ml Hoechst 33342 in phosphate buffered saline (PBS) 30 min later. Ten minutes later, the fluorescent intensity of each nucleus was quantitatively evaluated using a fluorescence microscope equipped with image-analysis software (IN Cell Analyzer 1000: GE Healthcare UK Ltd., Buckinghamshire, England).

2.7. Fluorescent labeling of PEG-PAsp(DET)

Alexa680-NHS (Invitrogen, Carlsbad, CA) was conjugated to the amino groups of PEG-PAsp(DET). PEG-PAsp(DET) was dissolved in 0.1 M $NaHCO_3$ at 4 °C, and an equimolar amount of Alexa680 in dimethylformamide (DMF) solution was added. After reacting for 3 h at 4 °C, the mixture was first dialyzed against an aqueous solution of 0.001 N HCl, and then against de-ionized water in dialysis tubing (MWCO: 12–14 kDa). The number of Alexa680 molecules conjugated to each PEG-PAsp(DET) molecule was determined to be 0.79 from the absorbance at 680 nm.

2.8. Fluorescence correlation spectroscopic (FCS) measurements of PEG-PAsp(DET)/CS mixtures

Alexa680-labeled PEG-PAsp(DET) solution at a concentration of 1 mg/ml and an equal volume of CS solution at varying concentrations was mixed and then diluted 30 times with PBS (pH 7.4) and MES buffer (pH 5.5) containing 20 mM MES and 150 mM NaCl, respectively. FCS measurements used a ConfoCor3 module (Carl Zeiss, Jena, Germany) equipped with a Zeiss C-Apochromat 40× water objective. A He–Ne laser (633 nm) was used for Alexa680-labeled pDNA excitation. For each sample, measurements were performed at room temperature with a sampling time of 20 s and repeated 10 times.

For the quantification of free PEG-PAsp(DET), a two-component model was applied to autocorrelation curves, where one component was free PEG-PAsp(DET) and the other was CS/PEG-PAsp(DET) complexes. When using this model, the diffusion times for free PEG-PAsp(DET) and CS/PEG-PAsp(DET) complexes were fixed. The diffusion time for CS/PEG-PAsp(DET) complexes was measured at CS:N = 1:1, because the diffusion time reached a plateau at a CS:N ratio of 0.5 at pH 7.4 and at a ratio of 1 at pH 5.5.

2.9. Förster resonance energy transfer (FRET) measurements

Double labeling of pDNA using fluorescein (ex/em = 492/518 nm) and Cy3 (550/570 nm) was done using Label IT Tracker Intracellular Nucleic Acid Localization Kits (Mirus) with a slightly modified protocol. The spectral properties of the pDNA were evaluated using a NanoDrop ND-3300 fluorospectrometer (NanoDrop Technologies,

Wilmington, DE) at an excitation of 470 nm with a blue LED. FRET efficiency was calculated from the relative emission ratio of Cy-3 (567 nm) to fluorescein (523 nm).

2.10. Size measurements of PMs by FCS

Plasmid DNA was labeled using Label IT Tracker Intracellular Nucleic Acid Localization Kits (Mirus, WI) following the manufacturer's protocol. The final DNA concentration was adjusted to 1.5 μg/ml. FCS measurements were performed as described previously. A He–Ne laser (633 nm) was used for Cy-5-labeled pDNA excitation.

2.11. Z-potential

Zeta potential was determined using a Zetasizer (Malvern Instruments, Worcestershire, U.K.) with a He–Ne Laser (λ = 633 nm) for the incident beam at a detection angle of 173° and at a temperature of 25 °C.

2.12. Intratracheal gene introduction into the lung

Mice were anesthetized by intraperitoneal administration of pentobarbital (60 mg/kg) (Kyoritsu Seiyaku, Tokyo, Japan). A microsprayer Model IA-1C-R (Penn Century, Philadelphia, PA) was placed into the trachea through the mouth, and then 50 μl of PM or CS-PM solution containing 6.7 μg pDNA was administered. Bronchoalveolar lavage (BAL) was performed with 500 μl PBS (instilled and recovered 4 times). LDH in BAL fluid was determined using a QuantiChrom Lactate Dehydrogenase Kit (BioAssay Systems, Hayward, CA) following the manufacturer's protocol. For mRNA measurements, lung tissue was extracted and total RNA was isolated using an RNeasy Mini Preparation Kit (Qiagen, Hilden, Germany) following the manufacturer's protocol. Gene expression was analyzed by real-time quantitative PCR using TaqMan Gene Expression Assays and an ABI Prism 7500 Sequence Detector. An IVIS™ Imaging System (Xenogen, Alameda, CA) was used to evaluate luciferase expression in the lung after intravenous injection of D-luciferin following the manufacturer's protocol.

2.13. Hydrodynamic gene introduction into skeletal muscle

Hydrodynamic gene introduction into skeletal muscle was performed as previously reported [12]. Briefly, after anesthetizing mice with 3% isoflurane (Abbott Japan Co., Ltd., Tokyo, Japan), a tourniquet was placed on the proximal thigh to transiently restrict blood flow. Then, from a distal site of the great saphenous vein, naked pDNA, PM, or CS-PM solution (375 μl) containing 50 μg pDNA was injected in 5 s. At 5 min after injection, the tourniquet was released. Blood samples were collected from the *vena cava* and allowed to stand overnight at 4 °C, followed by centrifugation to obtain serum. Serum CPK was determined using an Enzychrom Creatine Kinase Assay kit (BioAssay Systems) following the manufacturer's protocol. An IVIS™ Imaging System was used to evaluate luciferase expression in muscle after intravenous injection of D-luciferin.

3. Results and discussion

3.1. In vitro transfection with chondroitin sulfate

Cultured cell lines were transfected by PEG-PAsp(DET)/pDNA polyplex micelles (PMs) in the presence of chondroitin sulfate (CS). As the optimized charge ratio of PEG-PAsp(DET): pDNA is N:P = 80:1 [6,8], PEG-PAsp(DET)/pDNA/CS polyplex micelle systems (CS-PMs) were constructed by adding CS to PM solutions at the charge ratios of PEG-PAsp(DET): pDNA: CS (N:P:CS) = 80:1:10 and 80:1:100, in which the CS charge was calculated as the total number of carboxylate and sulfate residues. As shown in Fig. 1A, CS-PMs induced higher transgene expression in NIH3T3 cells than PMs alone. Other cell lines also showed similar enhancements in transgene expressions by the addition of CS, although the optimal amount of CS differed depending on the cell line (Supplementary Fig. 1). Interestingly, although the final transgene expressions improved with CS, an evaluation of the time-dependent change revealed that CS addition induced a delay in the time to achieve maximal transgene expression, which was in good agreement with the delayed profile in cellular uptake of CS-PMs (Fig. 1B, C).

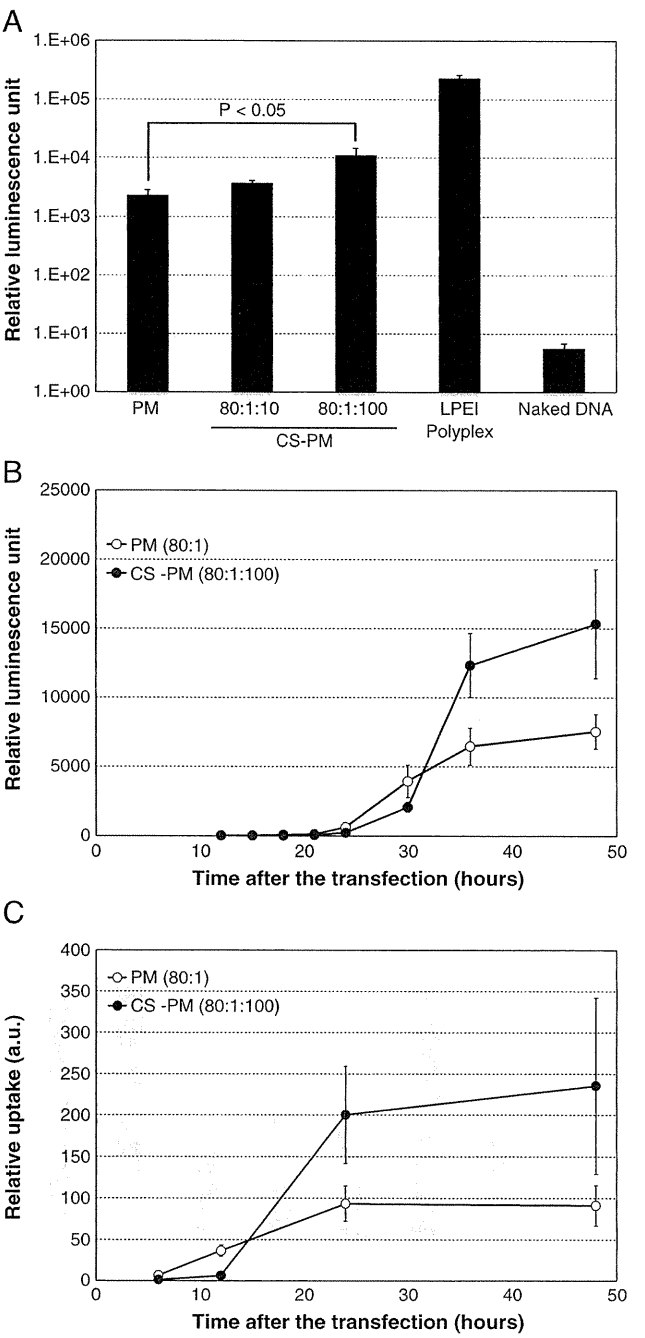

Fig. 1. Transfection efficiency in vitro. PM (N:P = 80:1), CS-PM (N:P:CS = 80:1:10 and 80:1:100), LPEI (N:P = 10:1) and naked DNA were transfected into NIH3T3 cells. A. Luciferase expressions after 48 h. B. Time-dependent profiles of luciferase expressions. C. Time-dependent profiles of pDNA uptake measured by quantitative PCR. Results are means ± SEMs (n = 5).

The PMs examined here, as well as most other polycation-based gene delivery systems, require an excess ratio of cationic polymers to pDNA for efficient transfection [6,8]. It is reasonable to assume that, at such a high N:P ratio, a considerable amount of PEG-PAsp(DET) exists in the free state without binding to PMs. Several reports have argued that free cationic polymers may be involved in endosomal escape and intracellular trafficking [13,14]. However, a critical issue is that these free polymers may induce toxic effects by interacting with cell membranes and other anionic biocomponents. It is possible that the anionic polycarbohydrate CS might abrogate such toxicity by associating with free polycations. Indeed, several recent studies that focused on the addition of polyanions, including CS, to polyplex systems showed enhanced transfection efficiency and reduced toxicity [15–20].

Accordingly, we analyzed the effect of CS on cell membrane integrity during *in vitro* transfection of PMs or CS-PMs. To assess cell membrane integrity, we used a DNA intercalator, YO-PRO1, which is impermeable to the normal cell membrane, but will permeate a membrane with perturbed integrity and emit a strong fluorescent signal due to DNA intercalation [21]. The fluorescent intensities of cultured cells due to permeated YO-PRO1 were quantitatively evaluated with a fluorescence microscope equipped with image-analysis software (IN Cell Analyzer 1000: GE Healthcare UK Ltd.).

At 30 min after transfection, the PMs formed at N:P = 80:1 induced an increase in fluorescent signals of YO-PRO1, suggesting enhanced cell membrane permeability (Fig. 2). In contrast, the PMs prepared at N:P = 3:1 showed almost no increase compared to the control. As reported previously, there was a substantial increase in the amount of free PEG-PAsp(DET) in the PM solution at an increased N:P [22]. Thus, it was reasonable to assume that the free PEG-PAsp(DET) in medium may have been involved in this significant increase in membrane permeability observed for the PM system at high N:P.

Indeed, addition of a corresponding amount of free PEG-PAsp (DET) into the medium induced as great an increase in fluorescence as the PMs prepared at N:P = 80:1, which was consistent with the previous assumption. Although polyplex from linear polyethyleneimine (LPEI) (N:P = 10), a commonly used transfectant, showed higher transfection efficiency than PMs or CS-PMs (Fig. 1A), the membrane damage and the cytotoxicity were notably observed for this system (Fig. 2 and Supplementary Fig. 2). In contrast, the membrane damage was substantially lowered in PEG-PAsp(DET) compared to PEI, indicating that the damage was sufficiently modest to have been effectively abrogated by the addition of CS. It should be noted that the enhanced cell membrane permeability was a transient, reversible phenomenon only at the initial phase of transfection, as it was not observed at 24 h after transfection (data not shown). Cell viabilities evaluated by an MTT assay at 48 h after transfection remained at nearly 100%, regardless of the presence or absence of CS (Supplementary Fig. 2).

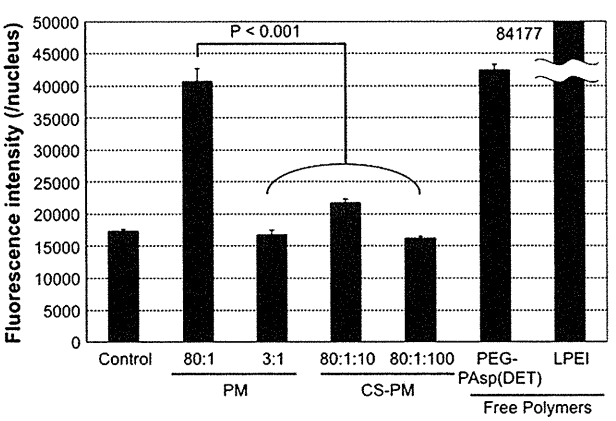

Fig. 2. Evaluation of membrane destabilization *in vitro*. PMs (N:P = 3:1 and 80:1), CS-PMs (N:P:CS = 80:1:10 and 80:1:100), and free PEG-PAsp(DET) and linear polyethyleneimine (LPEI)) with the same amine concentration as PMs (N:P = 80:1) were added to NIH3T3 cells, followed by treatment with YO-PRO1. The mean fluorescence intensity in cell nuclei was quantified for each well. About 3000 cells were analyzed in each well. Results are means of 3 wells ± SEMs.

3.2. Physicochemical characterization of CS-modulated polyplex systems

Next, we analyzed the effect of CS addition on the behaviors of free polycations as well as PMs. The reduced membrane damage after CS addition suggested that the amount of free polycations may have been substantially decreased in CS-PM solution due to the formation of polyion complexes between CS and excess PEG-PAsp(DET) in the medium.

Thus, to analyze the state of PEG-PAsp(DET) after mixing with varying ratios of CS, we measured the diffusion properties of Alexa680-labeled PEG-PAsp(DET) using FCS.

The diffusion time for PEG-PAsp(DET) reached a plateau at a CS:N ratio of 0.5:1, where the number of CS anionic charges was nearly equal to that of the PEG-PAsp(DET) cationic charges; approximately half of the amino groups in the 1,2-diaminoethane units in the side chain are protonated at pH 7.4 [9], suggesting the formation of a stoichiometric complex of CS and PEG-PAsp(DET) (Fig. 3). This result also suggested that there would be no free PEG-PAsp(DET) in the solution at CS:N ratios >0.5.

The formation of a stoichiometric complex around CS:N = 0.5:1 was also confirmed by measuring the z-potential (Supplementary Fig. 3). While the complex prepared at CS:N = 0.5:1 had a single fraction at around a neutral charge, the complex at CS:N = 1:1 had another fraction around −30 mV corresponding to free CS. Further, DLS measurements revealed that the CS/PEG-PAsp(DET) complex that was formed had a size of 43 nm with a narrow distribution of polydispersity index (PDI) = 0.13, indicating the formation of polyion complex micelles with a CS/PAsp(DET) core surrounded by a PEG shell. Of note is that the CS-PM system, even without free polycations, yielded a higher transfection efficiency than PM alone, as shown in Fig. 1A. We will return to this matter in a subsequent section of this paper.

Next, we examined the physicochemical properties of PMs with or without CS. For this purpose, we used a charge ratio of N:P = 20:1, because too great an excess of cationic polymers may interfere with precise analyses of the PMs characteristics. Because CS has an anionic nature, there may be a possibility of loosening the condensed structure of PMs [23]. The condensed state of DNA was analyzed by FRET measurements using DNA labeled with a pair of donor–acceptor fluorescent dyes on a single DNA molecule [24,25]. Of interest is that even with the addition of CS, there was no significant change in the

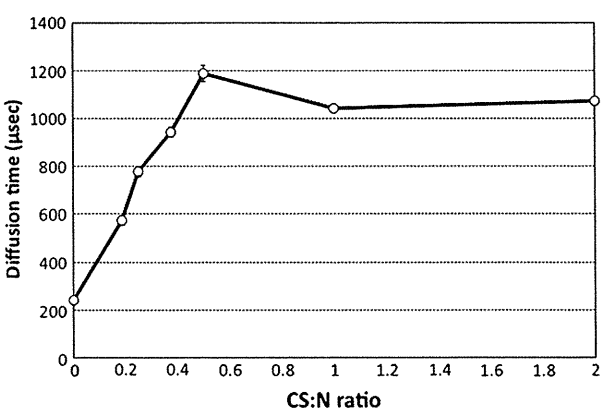

Fig. 3. Diffusion time measurements for Alexa680-labeled PEG-PAsp(DET) by FCS in the presence of varying amounts of CS in the solution. Results are means ± SDs.

condensation state of pDNA, suggesting that the disintegration of PM may not occur even in the presence of an appreciable amount of CS (Fig. 4). FCS using Cy5-labeled pDNA revealed that the diffusion time, which is proportional to particle diameter, showed a slight increase of approximately 1.3-fold after the addition of CS, suggesting some portion of CS may undergo the interaction with PMs (Fig. 5). The PMs z-potential became slightly negative after the addition of CS (+1.5 mV→−5.5 mV). These results suggested that the interaction of CS caused slight changes in the diameter and z-potential of PMs, although the PM structure with condensed pDNA in the core remained stable.

3.3. In vivo gene delivery into lung and skeletal muscle

To confirm the effect of CS for *in vivo* conditions, we performed transfection into mouse lung via intratracheal administration. To evaluate tissue damage, we quantified LDH released into bronchoalveolar lavage fluid (BALF) at 30 min after the administration. As shown in Fig. 6, CS significantly reduced LDH release to a level comparable to that of untreated mice. We also assessed the consequent tissue damage by quantifying the mRNA levels of pro-inflammatory cytokines in lung tissue at 24 h after administration. Although PMs induced a low, but detectable upregulation of TNF-α and Cox-2, CS addition significantly reduced the production of these cytokines (Fig. 7). Interestingly, the luciferase expressions evaluated by an IVIS Imaging System were comparable for these two systems with or without CS (Fig. 8).

Another *in vivo* approach is by using a hydrodynamic injection that targets skeletal muscle [12]. To assess toxicity, serum creatine phosphokinase (CPK) was determined at 4 h after injection. Using CS-PMs, the CPK level was significantly reduced compared to PMs, suggesting that CS also reduced the tissue damage in muscles (Fig. 9). In addition, CS-PMs yielded a higher and more prolonged transgene expression compared to PMs and naked pDNA, although there was no statistically significant difference among these 3 groups (Fig. 10). These *in vivo* results indicated that CS exhibited the favorable effects of ameliorating tissue damage and reducing the inflammatory response at the injection site without affecting the transfection competency of PMs.

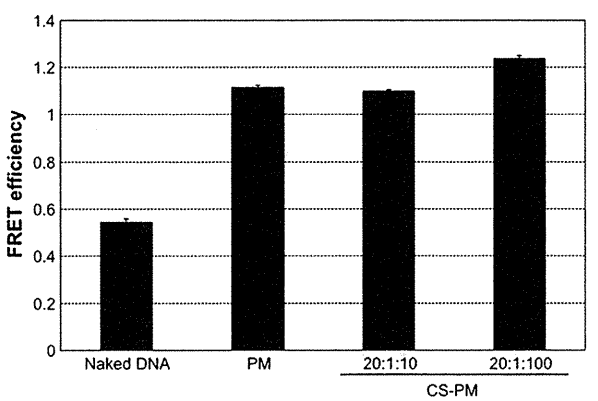

Fig. 4. Evaluation of pDNA condensation in the polyplexes by Förster resonance energy transfer (FRET). FRET efficiency between a pair of donor-acceptor fluorescent dyes (fluorescein and Cy3) tagged onto pDNA was determined for naked pDNA, PMs (N:P = 20:1), and CS-PMs (N:P:CS = 20:1:10 and 20:1:100). FRET efficiency is expressed as the emission intensity ratio of 567 nm (Cy3 emission) to 523 nm (fluorescein emission), where a higher value indicates a more condensed state of pDNA in the polyplexes. Results are means ± SDs (n = 3).

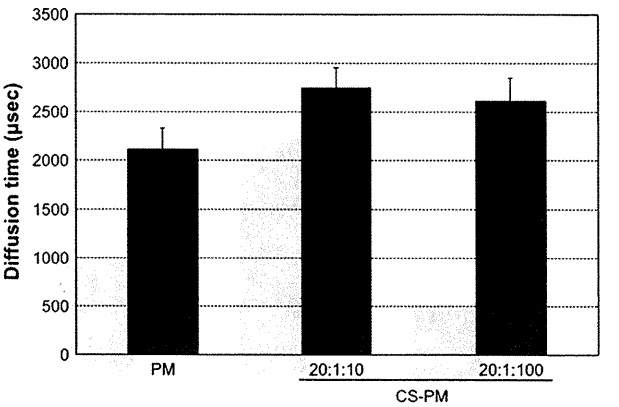

Fig. 5. Diffusion times for PMs (N:P = 20:1) and CS-PMs (N:P:CS = 20:1:10 and 20:1:100) measured by FCS. Results are means ± SDs.

3.4. Possible mechanisms for CS that improve the gene transfection efficacy of PM systems

The PM systems examined here consisted of a PEG-based block catiomer, PEG-PAsp(DET), which significantly reduced the cellular toxicity compared to polyplexes using non-PEGylated polycations [10,11]. Indeed, PM addition into the culture medium resulted in no decreases in cell viability as assessed by MTT assays (Supplementary Fig. 2). Nevertheless, a more sensitive assay to evaluate cell membrane integrity revealed that there was putative damage that increased membrane permeability, even though this was transient, and resulted in YO-PRO1 intercalated into chromosomal DNA to emit a fluorescent signal (Fig. 2). Worth noting is that this membrane damage was successfully abrogated by the addition of CS.

This was apparently due to neutralizing free polycations, the main component considered to cause membrane damage, in the medium via polyion complex formation. It is also worth noting that this propensity of CS to reduce membrane damage of the cultured cells caused by polycations is in line with the reduced adverse effects observed *in vivo*, including inflammatory cytokine production and tissue damage that induces LDH release. Thus, the use of CS in clinical settings is appealing for increasing the compliance of these PM systems. Although previous studies focused on the effects of anionic polycarbohydrates, such as hyaluronic acid (HA) and CS, on the behavior of cationic polylpexes [15–20], few of them addressed their roles in scavenging toxic free polycations.

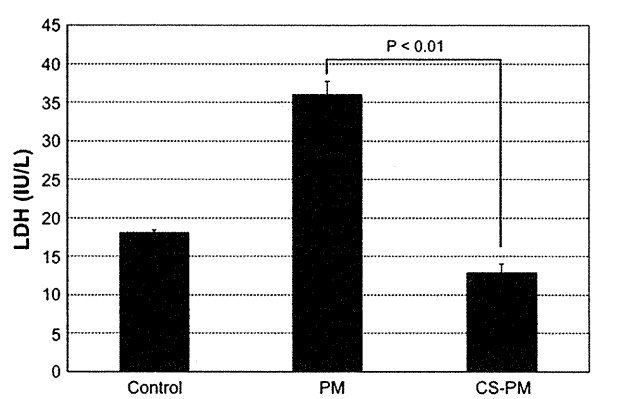

Fig. 6. LDH activity in bronchoalveolar lavage fluid (BALF). BALF was collected 30 min after the intratracheal administration of PMs (N:P = 20:1) and CS-PMs (N:P:CS = 20:1:100). Control indicates an untreated group. Results are means ± SEMs (n = 3).

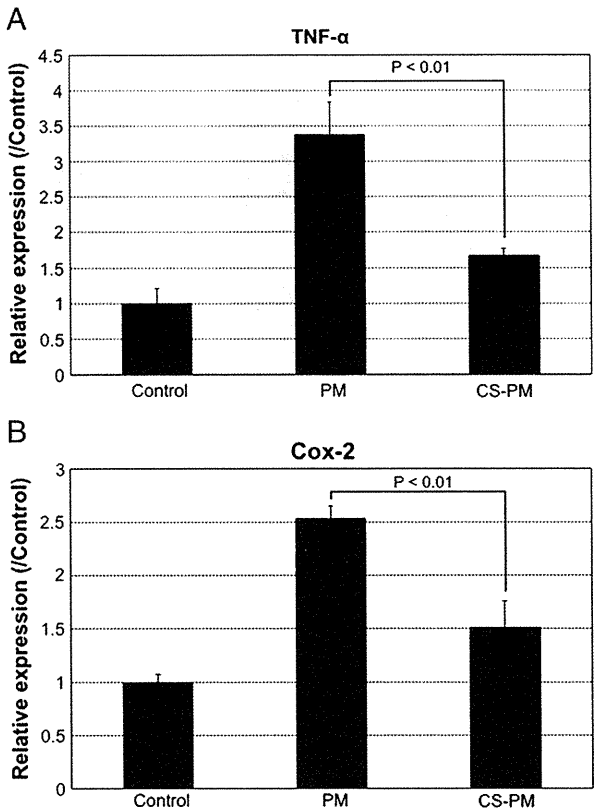

Fig. 7. Evaluation of pro-inflammatory cytokine (TNF-α and Cox-2) expression in lung tissue. PMs (N:P = 20:1) and CS-PMs (N:P:CS = 20:1:100) were administered intratracheally. Messenger RNA expression in lung was measured by quantitative polymerase chain reaction (PCR) at 24 h after administration. A. TNF-α, B. Cox-2. Results indicate relative values to untreated controls (means ± SEMs; n = 4).

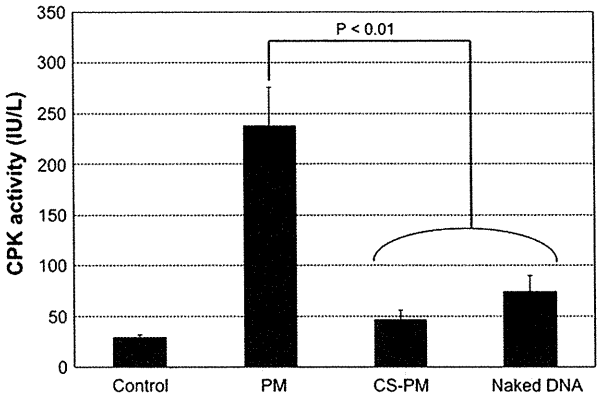

Fig. 9. Quantification of serum creatine phosphokinase (CPK). Serum was collected at 4 h after hydrodynamic injection of naked pDNA, PMs (N:P = 20:1), and CS-PMs (N:P:CS = 20:1:100). Control indicates an untreated group. Results are means ± SEMs (n = 5).

The primary reason for requiring excess polycations in their free form in the polyplex system is that these free polycations are assumed to be internalized into endosomes along with the polyplexes, thus facilitating their escape from endosomes to the cytoplasm by a proton sponge effect and/or direct perturbation of endosomal membranes. In any case, masking free polycations with CS via complexation is unfavorable for promoting endosomal escape, and is inconsistent with the observed preservation, or even improvement, in transfection efficacy of CS-PMs both *in vitro* and *in vivo*.

A plausible explanation for this controversial phenomenon is to assume a rearrangement of CS/PEG-PAsp(DET) complex micelles within endosomes that is synchronized with a pH drop to release free PEG-PAsp(DET). Note that, as shown in Fig. 3, CS/PEG-PAsp(DET) complex micelles have a charge stoichiometric composition of CS:N = 0.5:1 at pH 7.4. Thus, to maintain the charge stoichiometric regime, even at a lowered pH, there should be a liberation of a certain fraction of PEG-PAsp(DET) from the micelles. The pKa for the second protonation of the 1,2-diaminoethane unit of PAsp(DET) is 6.3 [9]. The endosomal pH, in turn, is reported to be ≈5.0–5.5, so that eventually PAsp(DET) in this pH range undergoes an additional protonation in the 1,2-diaminoethane unit, resulting in a shift in the charge stoichiometric ratio from CS:N = 0.5:1 to 1:1 and drives the liberation of PEG-PAsp(DET) from the micelles for charge compensation.

To estimate the pH responsive release of free PEG-PAsp(DET), we used FCS measurements for mixed solutions of CS and Alexa680-labeled PEG-PAsp(DET). As expected, a substantial amount of free PEG-PAsp(DET) was found at a CS:N = 0.5:1 at pH 5.5, which was consistent with the assumed liberation of PEG-PAsp(DET) from the complex micelles at the lowered pH conditions of the endosome

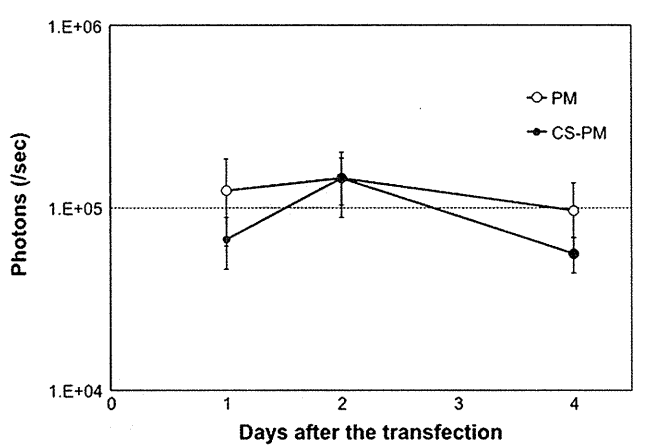

Fig. 8. Luciferase expressions in lung after intratracheal administration. PMs (N:P = 20:1;open circles) and CS-PMs (N:P:CS = 20:1:100; closed circles) loaded with a luciferase-expressing gene were administered intratracheally. The time-dependent profiles of luciferase gene expression were measured with an IVIS Imaging System. Results are means ± SEMs (n = 4).

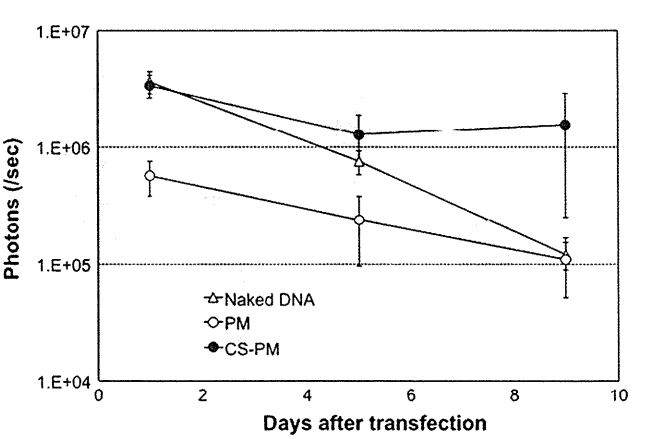

Fig. 10. Transfection efficacy in muscle after hydrodynamic injection. Naked pDNA (open triangles), PMs (N:P = 20:1; open circles), and CS-PMs (N:P:CS = 20:1:100; closed circles) were hydrodynamically injected into a hind limb muscle. The time-dependent profiles of luciferase gene expression were measured with an IVIS Imaging System. Results are means ± SEMs (n = 5).

(Supplementary Fig. 4). Worth noting is that the amount of free polymers became negligible at CS:N = 1:1 and pH 5.5, which supports the formation of a charge stoichiometric complex of CS with fully protonated PEG-PAsp(DET).

Consequently, from the above estimations, it is reasonable to conclude that the cellular uptake of CS/PEG-PAsp(DET) complex micelles along with CS-PMs enhances the endosomal escape of CS-PMs by releasing free PEG-PAsp(DET) in endosomes, leading to a high transfection efficiency.

4. Conclusions

The addition of CS to PEG-PAsp(DET)/DNA polyplex micelles abrogated membrane damage after *in vitro* and *in vivo* gene transfection. Effective complexation of CS with free polymers prevented the nonspecific binding to and the resulting destabilization of cell membranes. Further, CS/PEG-PAsp(DET) complex micelles co-localized in endosomes with CS-PMs selectively liberate free PEG-PAsp(DET) in the acidic compartment of the endosome, thereby facilitating the cytoplasmic translocation of CS-PMs and leads to effective gene expression. During *in vivo* gene transfer, CS remarkably reduced the inflammatory responses and tissue damage at the injection site. Thus, this system of PEG-PAsp(DET)/DNA polyplex micelles combined with CS shows promise for safe and practical gene transfer in future clinical settings.

Supplementary materials related to this article can be found online at doi:10.1016/j.jconrel.2011.04.026.

Acknowledgements

This work was financially supported in part by the Core Research Program for Evolutional Science and Technology (CREST) from Japan Science and Technology Corporation (JST) (K. K.), Grants-in-Aid for Scientific Research form the Japanese Ministry of Education, Culture, Sports, Science and Technology, Japan (MEXT) (K. I.), and Global COE Program "Medical System Innovationon through Multidisciplinary Integration" from MEXT, Japan. We thank Satomi Ogura, Yoko Hasegawa and Katsue Morii (The University of Tokyo) for technical assistance.

References

[1] S.C. De Smedt, J. Demeester, W.E. Hennink, Cationic polymer based gene delivery systems, Pharm. Res. 17 (2) (2000) 113–126.
[2] D. Schaffert, E. Wagner, Gene therapy progress and prospects: synthetic polymer-based systems, Gene Ther. 15 (16) (2008) 1131–1138.
[3] K. Itaka, K. Kataoka, Recent development of nonviral gene delivery systems with virus-like structures and mechanisms, Eur. J. Pharm. Biopharm. 71 (3) (2009) 475–483.
[4] S. Katayose, K. Kataoka, Water-soluble polyion complex associates of DNA and poly(ethylene glycol)-poly(L-lysine) block copolymer, Bioconjug. Chem. 8 (5) (1997) 702–707.
[5] K. Itaka, K. Yamauchi, A. Harada, K. Nakamura, H. Kawaguchi, K. Kataoka, Polyion complex micelles from plasmid DNA and poly(ethylene glycol)-poly(L-lysine) block copolymer as serum-tolerable polyplex system: physicochemical properties of micelles relevant to gene transfection efficiency, Biomaterials 24 (24) (2003) 4495–4506.
[6] N. Kanayama, S. Fukushima, N. Nishiyama, K. Itaka, W.D. Jang, K. Miyata, Y. Yamasaki, U.I. Chung, K. Kataoka, A PEG-based biocompatible block catiomer with high buffering capacity for the construction of polyplex micelles showing efficient gene transfer toward primary cells, ChemMedChem 1 (4) (2006) 439–444.
[7] K. Osada, H. Oshima, D. Kobayashi, M. Doi, M. Enoki, Y. Yamasaki, K. Kataoka, Quantized folding of plasmid DNA condensed with block catiomer into characteristic rod structures promoting transgene efficacy, J Am Chem Soc 132 (35) (2010) 12343–12348.
[8] K. Itaka, S. Ohba, K. Miyata, H. Kawaguchi, K. Nakamura, T. Takato, U.I. Chung, K. Kataoka, Bone regeneration by regulated in vivo gene transfer using biocompatible polyplex nanomicelles, Mol. Ther. 15 (9) (2007) 1655–1662.
[9] K. Miyata, M. Oba, M. Nakanishi, S. Fukushima, Y. Yamasaki, H. Koyama, N. Nishiyama, K. Kataoka, Polyplexes from poly(aspartamide) bearing 1,2-diaminoethane side chains induce pH-selective, endosomal membrane destabilization with amplified transfection and negligible cytotoxicity, J. Am. Chem. Soc. 130 (48) (2008) 16287–16294.
[10] K. Itaka, T. Ishii, Y. Hasegawa, K. Kataoka, Biodegradable polyamino acid-based polycations as safe and effective gene carrier minimizing cumulative toxicity, Biomaterials 31 (13) (2010) 3707–3714.
[11] M. Harada-Shiba, I. Takamisawa, K. Miyata, T. Ishii, N. Nishiyama, K. Itaka, K. Kangawa, F. Yoshihara, Y. Asada, K. Hatakeyama, N. Nagaya, K. Kataoka, Intratracheal gene transfer of adrenomedullin using polyplex nanomicelles attenuates monocrotaline-induced pulmonary hypertension in rats, Mol. Ther. 17 (7) (2009) 1180–1186.
[12] K. Itaka, K. Osada, K. Morii, P. Kim, S.H. Yun, K. Kataoka, Polyplex nanomicelle promotes hydrodynamic gene introduction to skeletal muscle, J. Control. Release 143 (1) (2010) 112–119.
[13] S. Boeckle, K. von Gersdorff, S. van der Piepen, C. Culmsee, E. Wagner, M. Ogris, Purification of polyethylenimine polyplexes highlights the role of free polycations in gene transfer, J. Gene Med. 6 (10) (2004) 1102–1111.
[14] J. Fahrmeir, M. Gunther, N. Tietze, E. Wagner, M. Ogris, Electrophoretic purification of tumor-targeted polyethylenimine-based polyplexes reduces toxic side effects in vivo, J. Control. Release 122 (3) (2007) 236–245.
[15] T. Ito, N. Iida-Tanaka, Y. Koyama, Efficient in vivo gene transfection by stable DNA/PEI complexes coated by hyaluronic acid, J. Drug Target. 16 (4) (2008) 276–281.
[16] T. Ito, N. Iida-Tanaka, T. Niidome, T. Kawano, K. Kubo, K. Yoshikawa, T. Sato, Z. Yang, Y. Koyama, Hyaluronic acid and its derivative as a multi-functional gene expression enhancer: protection from non-specific interactions, adhesion to targeted cells, and transcriptional activation, J. Control. Release 112 (3) (2006) 382–388.
[17] T. Ito, C. Yoshihara, K. Hamada, Y. Koyama, DNA/polyethyleneimine/hyaluronic acid small complex particles and tumor suppression in mice, Biomaterials 31 (10) (2010) 2912–2918.
[18] T. Kurosaki, T. Kitahara, S. Kawakami, K. Nishida, J. Nakamura, M. Teshima, H. Nakagawa, Y. Kodama, H. To, H. Sasaki, The development of a gene vector electrostatically assembled with a polysaccharide capsule, Biomaterials 30 (26) (2009) 4427–4434.
[19] A. Pathak, P. Kumar, K. Chuttani, S. Jain, A.K. Mishra, S.P. Vyas, K.C. Gupta, Gene Expression, Biodistribution, and Pharmacoscintigraphic Evaluation of Chondroitin Sulfate-PEI Nanoconstructs Mediated Tumor Gene Therapy, ACS Nano (2009).
[20] P. Xu, G.K. Quick, Y. Yeo, Gene delivery through the use of a hyaluronate-associated intracellularly degradable crosslinked polyethyleneimine, Biomaterials 30 (29) (2009) 5834–5843.
[21] P.T. Vernier, Y. Sun, M.A. Gundersen, Nanoelectropulse-driven membrane perturbation and small molecule permeabilization, BMC Cell Biol. 7 (2006) 37.
[22] M. Oba, K. Miyata, K. Osada, R.J. Christie, M. Sanjoh, W. Li, S. Fukushima, T. Ishii, M.R. Kano, N. Nishiyama, H. Koyama, K. Kataoka, Polyplex micelles prepared from omega-cholesteryl PEG-polycation block copolymers for systemic gene delivery, Biomaterials 32 (2) (2011) 652–663.
[23] M. Ruponen, S. Yla-Herttuala, A. Urtti, Interactions of polymeric and liposomal gene delivery systems with extracellular glycosaminoglycans: physicochemical and transfection studies, Biochim. Biophys. Acta 1415 (2) (1999) 331–341.
[24] K. Itaka, A. Harada, K. Nakamura, H. Kawaguchi, K. Kataoka, Evaluation by fluorescence resonance energy transfer of the stability of nonviral gene delivery vectors under physiological conditions, Biomacromolecules 3 (4) (2002) 841–845.
[25] K. Itaka, A. Harada, Y. Yamasaki, K. Nakamura, H. Kawaguchi, K. Kataoka, In situ single cell observation by fluorescence resonance energy transfer reveals fast intra-cytoplasmic delivery and easy release of plasmid DNA complexed with linear polyethylenimine, J. Gene Med. 6 (1) (2004) 76–84.

JACS
JOURNAL OF THE AMERICAN CHEMICAL SOCIETY

ARTICLE

pubs.acs.org/JACS

Odd–Even Effect of Repeating Aminoethylene Units in the Side Chain of N-Substituted Polyaspartamides on Gene Transfection Profiles

Hirokuni Uchida,[†] Kanjiro Miyata,[§] Makoto Oba,[∥] Takehiko Ishii,[†] Tomoya Suma,[†] Keiji Itaka,[§] Nobuhiro Nishiyama,[§] and Kazunori Kataoka*[,†,§,‡]

[†]Department of Bioengineering and [‡]Department of Materials Engineering, Graduate School of Engineering, The University of Tokyo, 7-3-1 Hongo, Bunkyo, Tokyo 113-8656, Japan

[§]Center for Disease Biology and Integrative Medicine, Graduate School of Medicine, The University of Tokyo, 7-3-1 Hongo, Bunkyo, Tokyo 113-0033, Japan

[∥]Department of Clinical Vascular Regeneration, Graduate School of Medicine, The University of Tokyo, 7-3-1 Hongo, Bunkyo, Tokyo 113-8655, Japan

Supporting Information

ABSTRACT: A series of the N-substituted polyaspartamides possessing repeating aminoethylene units in the side chain was prepared in this study to identify polyplexes with effective endosomal escape and low cytotoxicity. All cationic N-substituted polyaspartamides showed appreciably lower cytotoxicity than that of commercial transfection reagents. Interestingly, a distinctive odd–even effect of the repeating aminoethylene units in the polymer side chain on the efficiencies of endosomal escape and transfection to several cell lines was observed. The polyplexes from the polymers with an even number of repeating aminoethylene units (PA-Es) achieved an order of magnitude higher transfection efficiency, without marked cytotoxicity, than those of the polymers with an odd number of repeating aminoethylene units (PA-Os). This odd–even effect agreed well with the buffering capacity of these polymers as well as their capability to disrupt membrane integrity selectively at endosomal pH, leading to highly effective endosomal escape of the PA-E polyplexes. Furthermore, the formation of a polyvalent charged array with precise spacing between protonated amino groups in the polymer side chain was shown to be essential for effective disruption of the endosomal membrane, thus facilitating transport of the polyplex into the cytoplasm. These data provide useful knowledge for designing polycations to construct safe and efficient nonviral gene carriers.

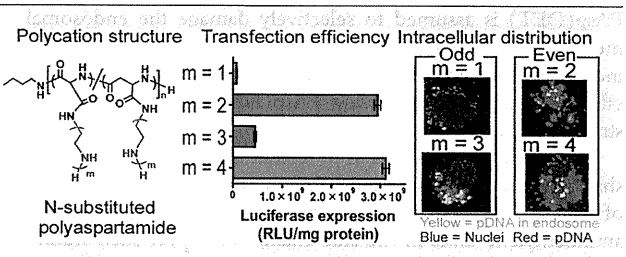

INTRODUCTION

Gene therapy has received considerable attention because of its significant potential to treat intractable diseases; however, the development of safe and efficient carriers of plasmid DNA (pDNA) remains a critical issue.[1,2] Among pDNA carriers, polyion complexes (PICs) formed between negatively charged DNA and polycations, which are termed "polyplexes", have been extensively studied.[3−8] Such polyplexes are required to stably deliver pDNA to the nuclei in the target cells. However, the most critical issue affecting the trafficking of polyplexes is the inefficient translocation from the endosomes to the cytoplasm after internalization through the endocytosis.[9] Hence, considerable efforts have been devoted to the development of polycations with potent endosomal escape ability.[10−15] However, such polycations often cause severe cytotoxicity.[16] Therefore, the fine-tuning the chemical structures of polycations to enhance their endosomal escape ability while cytotoxicity is reduced is a major key in designing polyplexes; this proves to be a challenge with respect to various fields of chemistry.

Linear polyethylenimine (linear PEI) is one of the most widely used polycations possessing potent endosomal escape ability.[17−20] Indeed, linear PEI polyplexes have been examined in several disease models to evaluate their clinical applications.[21] Linear PEI consists of repeating aminoethylene units and features a relatively low pK_a.[22] Hence, the protonation degree of linear PEI increases when pH decreases from the extracellular pH (~7.4) to the endosomal pH (~5.5). This facilitates the endosomal escape of linear PEI polyplexes because of endosomal disruption caused by increased osmotic pressure in the endosome (the so-called proton sponge effect[12,17]) and/or perturbation of the endosomal membrane caused by a direct interaction with polycations.[23−26] Thus, linear PEI exhibits a relatively high transfection efficiency but consequently induces considerable cytotoxicity because of interactions with biomolecules including the plasma membrane.[16,27] In order to solve this cytotoxicity problem, we have truncated a defined number of repeating aminoethylene units and introduced them into the side chain of the N-substituted polyaspartamides to obtain fine-tuned polycations achieving efficient gene transfection but reduced cytotoxicity. In our previous study,

Received: May 16, 2011
Published: August 31, 2011

dx.doi.org/10.1021/ja204466y | J. Am. Chem. Soc. 2011, 133, 15524–15532

Scheme 1. Synthesis of PAsp(EDA), PAsp(DET), PAsp(TET), and PAsp(TEP) by Aminolysis of PBLA

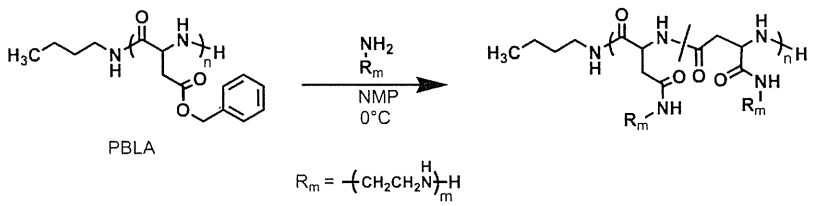

R_m = $-(CH_2CH_2NH)_m-H$

m = 1: PAsp(EDA), m = 2: PAsp(DET), m = 3: PAsp(TET), m = 4: PAsp(TEP)

poly{*N*-[*N*′-(2-aminoethyl)-2-aminoethyl]aspartamide} possessing two repeating aminoethylene units [$-(CH_2-CH_2-NH)_2-H$] was synthesized by the introduction of diethylenetriamine (DET) (bis(2-aminoethyl)amine) [PAsp(DET)] into the side chain of the N-substituted polyaspartamide.[28] PAsp(DET) showed minimal membrane destabilizing ability with a monoprotonated side chain at pH 7.4 but a potent membrane destabilizing effect with a diprotonated side chain at pH 5.5. Thus, PAsp(DET) is assumed to selectively damage the endosomal membrane, thus enabling less toxic gene transfer in various cells including fragile primary culture cells.[26] Furthermore, the in vivo efficacy of gene transfer using PAsp(DET) has been demonstrated in several disease models.[29,30]

These studies motivated us to further investigate the relationship between the protonation behavior and biological properties of the N-substituted polyaspartamides possessing repeating aminoethylene units in the side chain. We expect such studies to provide useful knowledge for designing polycations that are safe and efficient nonviral gene carriers. Therefore, in this study, we examined various N-substituted polyaspartamides possessing different numbers of repeating aminoethylene units in the side chain and evaluated the relationship between their protonated states at pH 7.4 and 5.5 and their biological properties such as the hemolytic activity, cytotoxicity, endosomal escape ability, and transfection efficiency. Interestingly, a distinctive odd–even effect associated with the number of aminoethylene units was observed on the efficiencies of endosomal escape and in vitro transfection. The polyplexes from the N-substituted polyaspartamides possessing even-numbered repeating aminoethylene units (PA-Es) achieved transfection efficiencies, without marked cytotoxicity, that were an order of magnitude higher than those from the N-substituted polyaspartamides possessing odd-numbered repeating aminoethylene units (PA-Os). The mechanism for endosomal escape of these N-substituted polyaspartamide polyplexes was examined in detail to explain this interesting odd–even effect.

RESULTS

Synthesis and Characterization of N-Substituted Polyaspartamides. Introduction of repeating aminoethylene units into the poly(β-benzyl-L-aspartate) (PBLA) side chain was performed by the aminolysis reaction of PBLA with ethylenediamine (EDA), diethylenetriamine (DET), triethylenetetramine (TET), or tetraethylenepentamine (TEP), as previously reported,[31] and we synthesized poly[*N*-(2-aminoethyl)aspartamide] [PAsp(EDA)], PAsp(DET), poly(*N*-{*N*′-[*N*″-(2-aminoethyl)-2-aminoethyl]-2-aminoethyl}aspartamide) [PAsp(TET)], and poly[*N*-(*N*′-{*N*″-[*N*‴-(2-aminoethyl)-2-aminoethyl]-2-aminoethyl}-2-aminoethyl)aspartamide] [PAsp(TEP)] (Scheme 1). It is noteworthy that in this way a series of N-substituted cationic polyaspartamides, with the same polymerization degree and molecular weight distribution, was readily obtained.[32] Each N-substituted cationic polyaspartamide is abbreviated as PAsp(R), in which R denotes the abbreviation of the amines substituted in the side chain. The quantitative aminolysis of the side chain was confirmed from the peak intensity ratio of the protons from the methyl group at the α-chain end of the polymer ($CH_3CH_2CH_2CH_2-$, δ = 0.9 ppm) to all the methylene protons in the side chains (δ = 2.7–3.6 ppm) in the ^{1}H NMR spectra (Figure 1).

pH-Dependent Change in the Degree of Protonation (α) of Amino Groups in the Side Chain of N-Substituted Polyaspartamides. In order to estimate the protonation states of the amino groups in the side chain of the N-substituted polyaspartamide (hereafter, the polymer), potentiometric titration was performed in the pH range 1.2–11.5 in a 150 mM NaCl solution at 37 °C. The resultant titration curves were converted to differential curves to determine each neutralization point (data not shown). The total molar amount of consumed NaOH in the titration of PAsp(EDA) and PAsp(DET) corresponded well to the residual molar amount of amino groups of each polymer (5 mmol) in the solution, indicating that all the amino groups of the polymer were protonated at the beginning (pH 1.2) and deprotonated at the end (pH 11.5). Accordingly, the degree of protonation (α) and pK (=pH + log[α/(1 − α)]) were calculated and plotted against pH and α, respectively (Figure 2). On the other hand, the molar amount of consumed NaOH for the titration of PAsp(TET) and PAsp(TEP) was substantially lower than the residual molar amount of amino groups in the solution, suggesting that the amino groups in PAsp(TET) and PAsp(TEP) should not be fully protonated, even at pH 1.2. Thus, the α/pH and pK/α curves of these polymers were calculated from the neutralization point in the differential curve and also shown in Figure 2. The change in the degree of protonation between pH 7.4 and 5.5 ($\Delta\alpha$), indicating the buffering capacity, was calculated for each polymer from the values of α at pH 7.4 and 5.5 and is summarized in Table 1. Obviously, PAsp(DET) showed the largest $\Delta\alpha$, followed by PAsp(TEP), PAsp(TET), and PAsp(EDA). The number of protonated amines in each polymer (NA) at the corresponding pH was also calculated from α and the number of residual amino groups in the polymer by the following equation: NA = $\alpha n \times 102$, where n is the repeating number of aminoethylene units in the polymer side chain and 102 is the averaged polymerization degree. Furthermore, the averaged cationic charge density (CD) of each polymer was defined as the ratio of the NA to the number-averaged molecular weight (M_n) of the polymers (Table 1). The pK_a values for each protonation step were determined from the pK/α curves and are summarized in Table 1. Note that the p$K_{a4,TEP}$ value was not determined because the fourth protonation of the residual amino

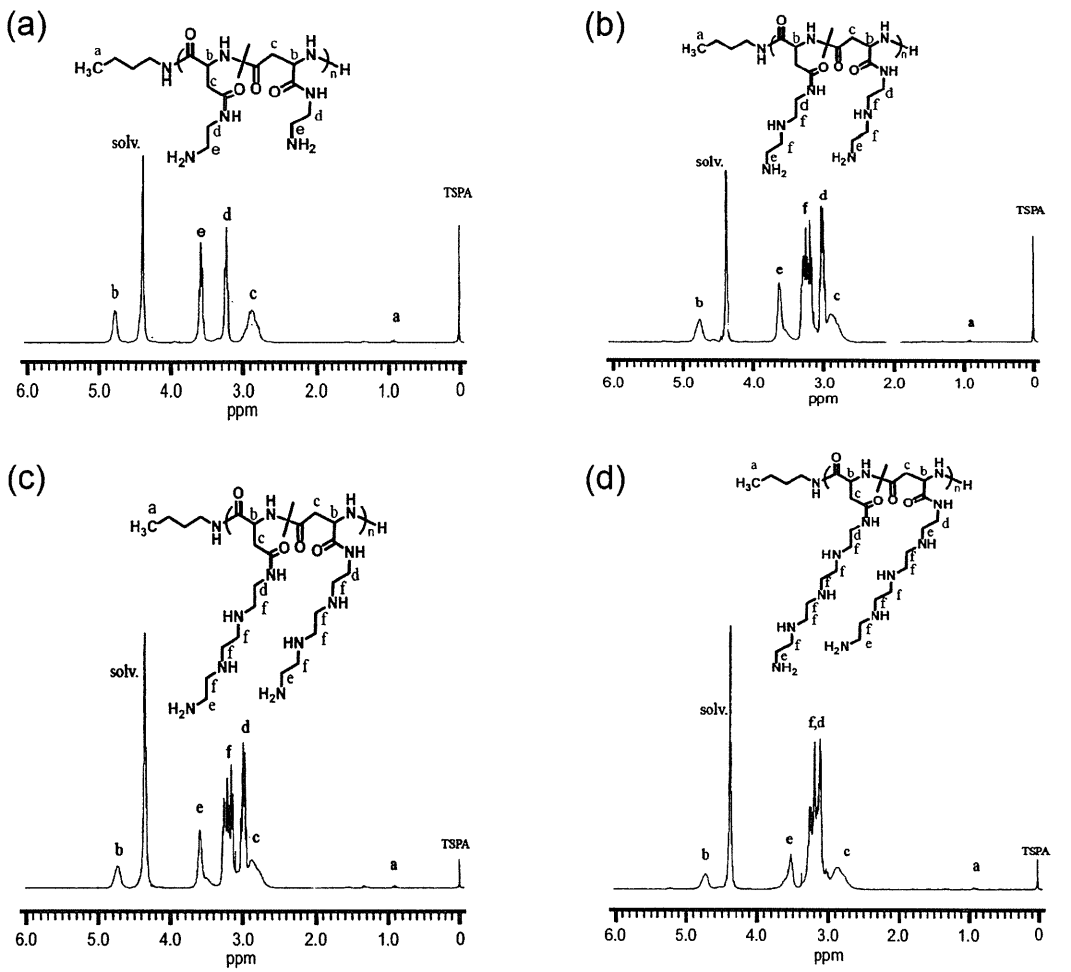

Figure 1. ^{1}H NMR spectra of (a) PAsp(EDA), (b) PAsp(DET), (c) PAsp(TET), and (d) PAsp(TEP). Solvent, D_2O; temperature, 70 °C; polymer concentration, 10 mg/mL.

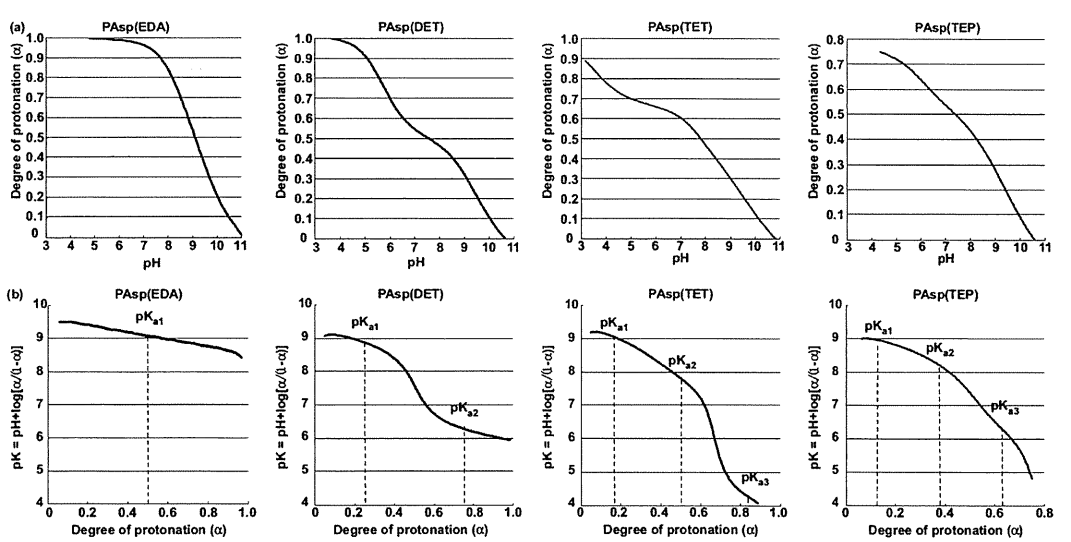

Figure 2. (a) α/pH curves and (b) pK_a/α curves of each N-substituted polyaspartamide in 150 mM NaCl solution at 37 °C.

dx.doi.org/10.1021/ja204466y | J. Am. Chem. Soc. 2011, 133, 15524–15532

Table 1. Physicochemical Parameters of the N-Substituted Polyaspartamides at pH 7.4 and 5.5

	α			number of protonated amines (NA[a])		charge density (CD[b])				
polymer	pH 7.4	pH 5.5	$\Delta\alpha$	pH 7.4	pH 5.5	pH 7.4	pH 5.5	pK_{a_1}	pK_{a_2}	pK_{a_3}
PAsp(EDA)	0.93	0.99	0.06	94	100	0.00538	0.00621	9.0		
PAsp(DET)	0.51	0.82	0.31	104	167	0.00505	0.00811	8.9	6.2	
PAsp(TET)	0.56	0.66	0.10	171	205	0.00682	0.00817	9.1	7.8	4.3
PAsp(TEP)	0.49	0.68	0.17	199	277	0.00673	0.00936	9.0	8.2	6.3

[a] NA = α × (the repeating number of aminoethylene units in the polymer side chain) × (the polymerization degree). [b] The ratio of the NA to the number-averaged molecular weight (M_n) of polymers.

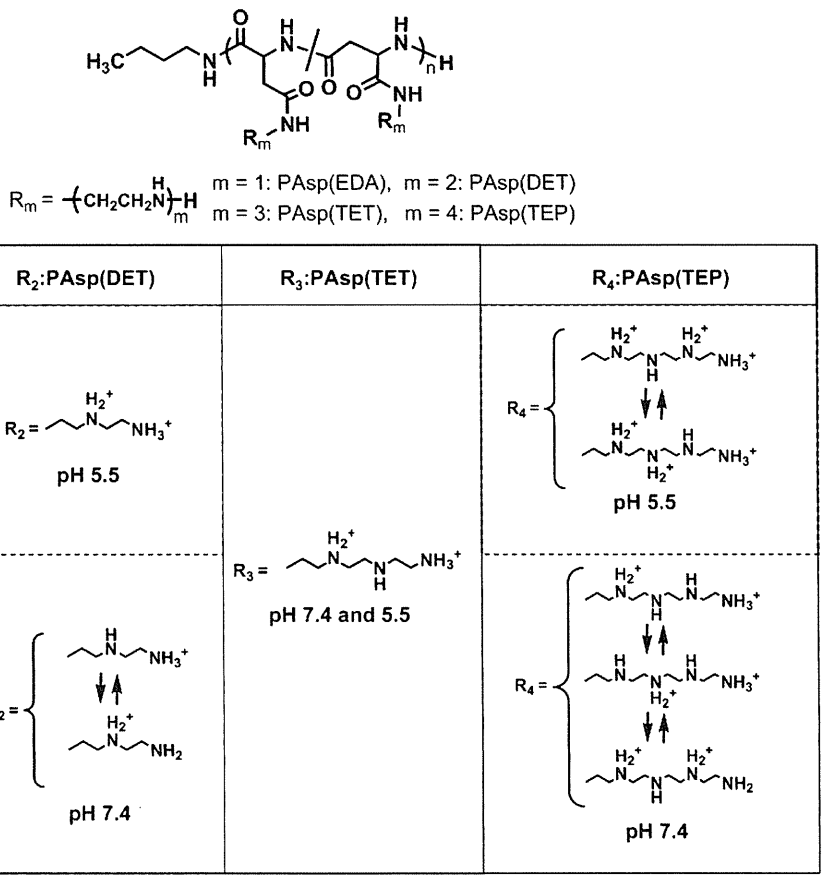

Figure 3. Major protonated structures of amino groups in the side chain of each polyaspartamide at pH 7.4 and 5.5.

groups in PAsp(TEP) was substantially limited, even at pH 1.2. Eventually, the major protonated structures of these polymers under physiological (pH = 7.4) and endosomal (pH = 5.5) conditions were estimated as shown in Figure 3.

Membrane Destabilizing Activity of N-Substituted Polyaspartamides. Our previous study revealed that PAsp(DET) disturbs the integrity of cellular membranes selectively at endosomal acidic pH presumably because of the transition of the side chain diamine unit from a monoprotonated to diprotonated state, which enhances the local charge density and facilitates the interaction with cellular membranes.[26] To determine the membrane-destabilizing activities of the N-substituted polyaspartamides as well as linear PEI (ExGen 500), the hemolysis assay was performed by mixing these polymers with murine erythrocytes at pH 7.4 and 5.5, at which extracellular neutral and endosomal acidic conditions, respectively, were simulated. As shown in Figure 4, ExGen 500 showed a considerably high hemolysis ratio (approximately 30%) at pH 7.4, which may be correlated with its high cytotoxicity. In contrast, all polymers induced substantially low hemolysis (less than 5%) at pH 7.4. Alternatively, at pH 5.5, the polymers possessing even-numbered repeating aminoethylene units [PAsp(DET) and PAsp(TEP)] and ExGen 500 significantly enhanced the hemolytic activity, whereas those possessing odd-numbered repeating units [PAsp(EDA) and PAsp(TET)] showed no significant increase. Thus, a unique odd–even effect of the repeating number of aminoethylene units was clearly observed for the pH-dependent hemolytic activity of a series of N-substituted polyaspartamides. Furthermore, the hemolytic